

SMALL SCALE MODELING OF HYDRODYNAMIC FORCES IN PRESSURE SUPPRESSION SYSTEMS

Final Report

W. G. Anderson P. W. Huber
A. A. Sonin

Massachusetts Institute of Technology

POOR ORIGINAL

1776 213

Prepared for
U. S. Nuclear Regulatory Commission

7912200856

NOTICE

This report was prepared as an account of work sponsored by the United States Government. Neither the United States nor the United States Nuclear Regulatory Commission, nor any of their employees, nor any of their contractors, subcontractors, or their employees, makes any warranty, express or implied, nor assumes any legal liability or responsibility for the accuracy, completeness or usefulness of any information, apparatus, product or process disclosed, nor represents that its use would not infringe privately owned rights.

POOR ORIGINAL

Available from
National Technical Information Service
Springfield, Virginia 22161
Price: Printed Copy \$5.25 ; Microfiche \$3.00

1775 214

The price of this document for requesters outside of the North American Continent can be obtained from the National Technical Information Service.

SMALL SCALE MODELING OF HYDRODYNAMIC FORCES IN PRESSURE SUPPRESSION SYSTEMS

Final Report

W. G. Anderson P. W. Huber
A. A. Sonin

Manuscript Completed: December 1977
Date Published: March 1978

Department of Mechanical Engineering
Massachusetts Institute of Technology
Cambridge, MA 02139

Prepared for
Division of Reactor Safety Research
Office of Nuclear Regulatory Research
U. S. Nuclear Regulatory Commission
Under Contract No. NRC-04-77-011

1776 215

TABLE OF CONTENTS

	Page
Abstract	1
Nomenclature	3
1. INTRODUCTION	5
2. THE MODELING LAWS	8
3. EXPERIMENTS	19
4. RESULTS AND DISCUSSION	24
4.1 Typical Pressure Histories	24
4.2 Verification of the Scaling Laws	25
4.3 Effect of Excessive Vapor Pressure in Small-Scale Tests	30
4.4 On the Precautions That Must be Taken to Avoid Pool Oscillations due to Gas in the Liquid	32
5. CONCLUSIONS	35
References	37
Figures	38

Abstract

Experiments were conducted to test the validity of the scaling laws which have been put forward for the small-scale modeling of the air clearing phase of flow into the condensation pool of a pressure suppression system. Three geometrically similar wetwells (differing in linear dimension by a factor of 4) were used, along with two liquids (differing in density by a factor of three) and three gases (differing in enthalpy by a factor of ten). When using different pressures, liquids, and gases, the dimensionless pressures were in excellent agreement as long as the four scaling parameters were held constant. The enthalpy flux must be scaled by the use of an orifice to ensure that the pressures will scale.

Our tests uncovered two areas where the scaling laws will not hold if the proper precautions are not taken. The vapor pressure of the liquid must be kept quite low. If water is used it must be cooled to near freezing when the system size is less than about 1:10 scale of a system with pressures near atmospheric. It is also possible to avoid this problem by using a liquid with a low vapor pressure, such as Meriam manometer fluid.

Peak downloads will scale only if the containment walls are rigid and precautions are taken to eliminate small air bubbles in the liquid. The problem with the air bubbles can be eliminated by adding a surfactant or by using a particular wetwell fluid (such as Meriam manometer fluid). If these precautions are taken, the scaling laws originally put forward by Moody are valid.

1775 217

NOMENCLATURE

C_m	mass flow coefficient through orifice (dimensionless)
d	downcomer diameter (m)
d_i	orifice internal diameter (m)
D	wetwell diameter (m)
g	acceleration due to gravity ($9.8 \text{ m}\cdot\text{sec}^{-2}$)
G	equivalent mass flux density through the orifice ($\text{kg}\cdot\text{m}^{-2}$)
h_D	specific stagnation enthalpy of drywell gas (J/kg)
P	pressure at a given point (kPa)
$P(0)$	initial pressure prior to blowdown at a given point (kPa)
P_1 to P_4	pressures from transducers 1 to 4 (Fig. 2) (kPa)
P_D	drywell pressure (kPa)
P_w	<u>initial</u> wetwell pressure (kPa)
P^*	dimensionless pressure at a point, Eq. (14)
R	specific gas constant (universal gas constant divided by molar mass of gas) ($\text{J}/^\circ\text{K}\cdot\text{kg}$)
Re	a Reynolds number for gas flow through the orifice, Eq. (5) (dimensionless)
t	time measured from the initiation of blowdown (sec)
t^*	dimensionless time = $t\sqrt{g/D}$
T_D	drywell gas absolute temperature ($^\circ\text{K}$)
v	velocity at a given point ($\text{m}\cdot\text{sec}^{-1}$)
v^*	dimensionless velocity = v/\sqrt{gD}
V	total volume of wetwell system downstream of orifice (m^3)

- γ ratio of specific heats of drywell gas (dimensionless)
- μ_D viscosity of drywell gas ($\text{kg}\cdot\text{m}^{-1}\text{t}^{-1}$)
- π_1 to π_4 dimensionless scaling parameters [Eqs. (7)-(11)]
- ρ density of wetwell liquid ($\text{kg}\cdot\text{m}^{-3}$)
- ρ_D density of drywell gas ($\text{kg}\cdot\text{m}^{-3}$)
- τ rise time for pressure in empty wetwell (used for orifice calibration) (sec)

1. INTRODUCTION

During the past two years, considerable work has been done to establish a proper design basis for the hydrodynamic loads in the water-type pressure suppression containment of systems of boiling water reactors (BWR's). Three generations of such systems have been developed by the General Electric Company: Marks 1, 2, and 3. In early 1975, during the testing by G.E. of the Mark 3 systems, it became apparent that certain loads had not been adequately considered in the two earlier designs. At that time, there were 25 BWR reactors with Mark 1 containments in the United States, 19 of them operational, and several reactors with Mark 2 containments in advanced construction stages. A strong research and testing program was immediately mounted by the nuclear industry and the Nuclear Regulatory Commission to resolve the problem as quickly as possible.^{1,2}

Of major concern in the Mark 1 containment were the forces which would be exerted on the containment during the initial stages of a loss-of-coolant accident (LOCA), when the air in the drywell and vent system is displaced by the steam from the (postulated) pipe rupture and ejected into the wetwell of the containment system. This causes at first a sharp downward force on the wetwell floor as the vents clear of water, and then an upward load on the wetwell as the air trapped over the water is over-compressed by the rapid upheaval of the condensation pool ("pool swell"). The pool swell also causes impact loads on the internal structures of the wetwell.

The pool swell process is a complex one, for geometrical and other

reasons, and at present the most acceptable method of predicting the loads is through small-scale experimental modeling, using scaling laws to extrapolate the small-scale results to full-scale conditions. This is the approach that G.E. took in 1975, when they began simulating the air expulsion stage of LOCA's in a 1/12-scale model of a typical Mark 1 containment. Their model actually represented only a two-downcomer, 7.5° segment of the full 360° Mark 1 containment torus. The following year, the nuclear industry sponsored further tests in a similar 1/4-scale model, and NRC funded the Lawrence Livermore Laboratory to carry out tests in a more elaborate 1/5-scale model of a 90° segment of the Mark 1 torus. The industrial tests are completed and analyzed. However, much of the data remains in proprietary form. The Livermore tests are finished and the data should soon become available.

The method of small-scale modeling rests on a knowledge of the scaling laws which ensure that dynamic similarity exists between the model and the full-scale system and which enable one to extrapolate the data derived from the model to full-scale conditions. Because of the complexity of the pool swell process, it turns out to be impossible or impractical to achieve exact dynamic similarity between a small-scale system and a full-scale one. However, by invoking a simplified but nevertheless realistic model of the actual pool swell process, F.J. Moody of G.E.³ was able to suggest a sufficiently simple set of modeling laws to allow convenient small-scale modeling. These laws are the basis for the industry's small-scale tests. The simplifying assumptions on which the modeling laws are based are reasonable, but

fundamental experimental checks of the laws are nevertheless required.

This paper will describe a series of direct experimental tests of the modeling laws for the early period of blowdown into the condensation pool when the gas being ejected from the drywell is mostly air and condensation is negligible. The scaling laws are tested in geometrically similar, drum-shaped "wetwell" test-sections with a single downcomer. The geometry is not intended to precisely simulate any particular existing containment system. However, the major geometrical parameters are approximately similar to a G.E. Mark 1 system. The present paper is a complete description of the work which was reported in part in Reference 4.

1776 222

2. THE MODELING LAWS

In what follows we shall quickly derive the scaling laws for the pool swell process. The approach follows Moody's,³ but is somewhat more rigorous in its consideration of the effect of the vent system's hydraulic resistance.

Consider a set of geometrically similar rigid systems, like the one in Fig. 1, consisting of a closed wetwell, partly filled with liquid, connected to a drywell by one or several downcomer pipes. Geometrical similarity includes the initial liquid level as well as the fixed features. At $t \leq 0$, the pressure in the wetwell and downcomer gas spaces is P_w , and the liquid is stationary. At $t > 0$, the enthalpy h_D and the pressure P_D in the drywell increase rapidly with time.

We are interested in the scaling laws for the pressure distribution in the wetwell and the velocity distribution of the wetwell liquid. To understand what these quantities depend on, we consider the following simplified model of the actual pool swell process. First, we shall assume (for the time being) that the pressure drop which occurs in the downcomer during flow is largely localized; that is, it occurs primarily at one given location in the downcomer, at the "orifice." Next, we note that the process involves three separate fluid regions: the region I of gas which is bounded by the orifice on the upstream side and the liquid on the other; the region II of liquid; and the region III of trapped gas in the wetwell. We shall assume that in regions I and III the gases are perfect and noncondensable and the pressure uniform (inertial effects

occur primarily in the liquid, not in the gas, and acoustic times are short compared with the characteristic blowdown times). As for the liquid, we assume that its motion is incompressible and inviscid. (Acoustic times in the liquid are also very short, and the Reynolds number very large.) After the bubble is formed, we assume that it will drive the pool motion. Heat transfer is neglected between the liquid and the gas, and between the gas and the wetwell structure. Interfacial surface tension effects are assumed to be negligible.

Based on this simplified model of the process, we can deduce that the pressure at a given point in the system must have the dependence

$$P = P(P_w, \rho, g, D, \gamma, h_D G, t) , \quad (1)$$

where $h_D G$ is the instantaneous enthalpy flux density associated with the flow of gas through the orifice, expressed as an enthalpy flow rate per unit downcomer area. h_D is the drywell gas enthalpy, and G is the equivalent mass flux density through the orifice. The other symbols are defined in the Nomenclature. (If γ is different in regions I and III, both values of γ must be inserted.) An entirely similar dependence applies to the velocity at a given point. That $\rho, g, D,$ and t must enter Eq. (1) is obvious because the pressure and velocity distributions depend on the dynamics of the liquid pool. P_w and γ enter through the isentropic pressure-volume relation for the trapped gas, which controls the boundary condition for the region III side of the liquid. The additional quantity $h_D G$ represents the enthalpy flux into region I. This quantity enters because it appears [in addition

to some of the other variables in Eq. (1)] in the energy equation for region I, and the energy equation controls the pressure-volume relation for region I and therefore the boundary condition for the side of the liquid.

Note that h_D and G do not appear separately in Eq. (1), but only as a product. This is so because the region I mass conservation law, which involves G separately, does not affect the pressure-volume relation for the region. The pressure-volume relation is controlled by the energy equation alone. The mass conservation law controls the gas density in region I, but the gas density plays no role here because inertial effects in the gas phases are neglected and heat transfer is absent. It is precisely because h_D and G appear only as a product, but not individually, that it is possible to derive a sufficiently simple set of modeling laws.

Applying straightforward dimensional analysis, we deduce from Eq. (1) that a dimensionless pressure like $(P - P_W)/P_W$ must have the dependence

$$\frac{P - P_W}{P_W} = f \left(\frac{P_W}{\rho g D}, \gamma, \frac{h_D G(t)}{\rho g^{3/2} D^{3/2}}, t\sqrt{g/D} \right). \quad (2)$$

A dimensionless velocity like v/\sqrt{gD} has a similar dependence. The implicit assumption, of course, is that we are referring to the pressure or velocity at a particular spot in the system; otherwise, a dependence on position must be included.

Equation (2) implies that if $P_W/\rho g D$ and γ are the same in two

ASS 8717

geometrically similar systems--a full-scale prototype and a small-scale model, say--and if $h_D G / \rho g^{3/2} D^{3/2}$ is the same in both at corresponding values of the dimensionless time $t\sqrt{g/D}$, then the dimensionless pressure (and velocity) will be the same in both at corresponding values of $t\sqrt{g/D}$.

This recipe for modeling is simple. However, there is still a practical difficulty: one must know how to ensure that $h_D G / \rho g^{3/2} D^{3/2}$ is the same in the model as in the prototype.

We address this last problem by considering the scaling laws for the flow through a standard orifice or any flow restriction in a pipe system, set between an upstream point where the pressure P_D is specified (in Fig. 1, the drywell) and a downstream point where the pressure is P (in Fig. 1, the region I). We consider the set of geometrically similar restrictions in a pipe of diameter d (the downcomer), and we assume that the region where the pressure drop occurs is sufficiently localized that the flow there can be considered quasi-steady. We can then show from dimensional considerations that a dimensionless mass flux density, which we shall call the mass flow coefficient C_m , in analogy to the discharge coefficient C_d for volume flow in nozzles,[†]

$$C_m \equiv \frac{G}{\rho_D \left[\frac{2(P_D - P)}{\rho_D} \right]^{1/2}} \quad (3)$$

[†]Note that by this definition the pressure drop $P_D - P$ is equal to C_m^{-2} times the dynamic pressure, $\frac{1}{2}\rho_D v^2$, based on the drywell gas density and the velocity in the downcomer. Thus, C_m^{-2} is a sort of total head loss coefficient for the downcomer, including both the viscous loss as well as the inviscid Bernoulli pressure drop.

must have the functional form

$$C_m = C_m \left(\frac{d_i}{d}, \frac{P_D - P}{P_D}, \gamma, Re \right) \quad (4)$$

Here, ρ_D is the gas density at the upstream station, d_i is the diameter of the standard orifice, and

$$Re \equiv \frac{\sqrt{\rho_D P_D} d}{\mu_D} = \frac{P_D d}{\mu_D \sqrt{RT_D}} \quad (5)$$

is a characteristic Reynolds number for the flow (see the Nomenclature for the symbols). The dependence on d_i/d in Eq. (4) is written for the particular case where the resistance is a standard orifice. More generally, the form of Eq. (4) would simply depend on the geometry of the restriction.

In terms of the mass flow coefficient introduced in Eq. (3), we can write

$$\frac{Gh_D}{\rho g^{3/2} D^{3/2}} = \sqrt{2} \frac{\gamma}{\gamma-1} \frac{P_D}{P_W} \frac{P_W}{\rho g D} \left[1 - \frac{P_W}{P_D} - \frac{P_W}{P_D} \left(\frac{P-P_W}{P_W} \right) \right]^{1/2} C_m \left(\frac{RT_D}{gD} \right)^{1/2} \quad (6)$$

Now, we have seen that if γ and $P_W/\rho g D$ are the same in the model and prototype systems, similarity will be achieved--that is, $(P-P_W)/P_W$ will be the same in both systems at corresponding values of dimensionless time $t\sqrt{g/D}$ --if $Gh_D/\rho g^{3/2} D^{3/2}$ is also the same at corresponding $t\sqrt{g/D}$. From Eq. (6) we see that this condition is satisfied if P_D/P_W and $C_m (RT_D/gD)^{1/2}$ are the same in both systems

055 0771

1776 227

at corresponding values of dimensionless time $t\sqrt{g/D}$. According to Eq. (4), on the other hand, C_m depends on dimensionless time only via the dimensionless pressure ratio $(P_D - P)/P_D$. Hence, $C_m(RT_D/gD)^{1/2}$ will be the same in both systems at corresponding dimensionless times if it is the same at corresponding values of $(P_D - P)/P_D$.

Our conclusion, then, is that the proper modeling laws for pool swell are that

$$\pi_1 \equiv \gamma \quad (7)$$

and

$$\pi_2 \equiv \frac{P_w}{\rho g D} \quad (8)$$

be the same in the model and the prototype system, that

$$\pi_3 \equiv \frac{P_D}{P_w} \quad (9)$$

be the same in the model and prototype system at corresponding values of

$$t^* \equiv t\sqrt{g/D}, \quad (10)$$

and that

$$\pi_4 \equiv C_m \left(\frac{RT_D}{gD} \right)^{1/2} \quad (11)$$

be the same in the model as in the prototype system at all values of the dimensionless pressure drops $(P_D - P)/P_D$ encountered in the process. It then follows that a dimensionless pressure like $(P - P_w)/P_w$, or dimensionless velocity like v/\sqrt{gD} , at any given point will be the

same in the model as in the prototype. In general, the dimensionless quantities will have the form

$$\frac{P - P_w}{P_w} \text{ or } \frac{v}{\sqrt{gD}} = f(\pi_1, \pi_2, \pi_3, \pi_4, t^*) \quad (12)$$

The modeling procedure is thus the following:

- (a) Make the model geometrically similar to the prototype, including the location, but not the magnitude, of the flow restriction in the downcomer.
- (b) Adjust π_4 in the model to that of the prototype system by increasing the resistance (for example, by using an orifice in the line) so as to balance the effect of the smaller D [see Eq. (11)]. This can be done after several orifices with different d_i 's have been calibrated at their design Re 's [see Eq. (4)] over the range of $(P_D - P)/P_D$ expected in the blowdown process. One should try to ensure, by trial and error, that π_4 is approximately the same in both systems over the whole excursion in $(P_D - P)/P_D$.
- (c) Use the same values of π_1 and π_2 in the model as in the prototype, and the same applied pressure history $\pi_3(t^*)$.
- (d) Measure $P^* = (P - P_w)/P_w$ and $v^* = v/\sqrt{gD}$ versus t^* in the model, and calculate P and v for the prototype from the knowledge that P^* and v^* are the same in both systems at geometrically corresponding locations and t^* .

1775 229

888 2771

The development given above has assumed that the flow resistance in the downcomer is localized, that is, it occurs primarily at a known station. This situation is in fact approximated fairly well in the tests which are described in what follows. Actual containment systems, however, are more complex, and the question arises whether this introduces complications into the modeling. Is only the total flow resistance important, or must one also be concerned with the actual distribution of the resistance in the line?

It should be emphasized that in steady or quasi-steady adiabatic flow it makes no difference to the downstream pressure or the enthalpy flux whether the flow resistance is localized, or distributed in various parts of the piping system. Only the overall effect counts. In unsteady flow, however, there may be some difference since the distribution of the resistance in the line affects the time it takes the pipe system to fill up in response to an increased driving pressure. As to how this might affect the modeling, we make the following remarks.

(1) In a real containment system, the flow resistance occurs (to a good approximation) in a series of "discrete" locations in the vent system: at the entrance, at bends, area reductions, tees. By applying the energy equation to each uniform-pressure region between successive restrictions, one can easily show that completely accurate modeling should be achieved if in the model the vent system geometry is identical to that of the prototype, but each discrete flow resistance is scaled so as to make the local π_4 the same in both systems.

(2) If the vent system geometry is faithfully modeled, but the

main flow restriction is further downstream in the model than in the prototype--as would occur, for example, if a single orifice in the downcomer were used in the model to bring the model's π_4 to the prototype value--then one would expect that the model would, if anything, tend to show a more violent vent clearing and pool swell than the prototype. This is so because the vent system would tend to follow the rising drywell pressure faster than the properly scaled value so that at a given dimensionless time, the dimensionless driving pressure would tend to be higher in the model than in the prototype system. The modeling would thus tend to be conservative.

(3) If the vent in the model system is not geometrically scaled, but has a smaller volume than the scaled one, and if the total flow resistance is properly scaled so that π_4 is the same in the model as in the prototype, but the model's flow resistance is localized at a point near to the vent exit, then the model should again, if anything, tend to have a more violent vent clearing and pool swell than the prototype. The reason is the same as that given above.

One might stress, in concluding this section, that if h_D and G had appeared individually in Eq. (1) rather than as a product, we would have found that instead of π_4 there would be two modeling parameters, $\pi_4' = C_m$ and $\pi_5 = (RT_D/gD)^{1/2}$. If one had to make π_5 the same in a small-scale system as in a large one, modeling would be very difficult because the gas enthalpy would have to be scaled with system size. This difficulty is removed only if one recognizes, as Moody did,³ that it is merely the product $h_D G$ that appears in Eq. (1). As a result, only the

product π_4 of C_m and $(RT_D/gD)^{1/2}$ must be scaled, and this can be done relatively easily by adjusting the line discharge coefficient C_m .

1775 232

1112-522

TABLE 1. Geometric Parameters of Wetwell Test System

$$\frac{\text{downcomer area}}{\text{pool area}} = 0.033$$

$$\frac{\text{liquid depth}}{\text{downcomer diameter}} = 6$$

$$\frac{\text{submergence}}{\text{downcomer diameter}} = 2$$

$$\frac{\text{wetwell gas volume}}{\text{liquid volume}} = 1$$

3. EXPERIMENTS

The scaling laws were verified experimentally in the somewhat simplified "containment system" geometry system shown in Fig. 2. The wetwell was a simple cylindrical vessel of internal diameter D . A single downcomer with internal diameter $d = 0.182D$ and length $2.73D$ entered the wetwell from the top center. The top of the downcomer opened directly into a "drywell" which in our tests was simply a reservoir with a volume large compared with that of the airspace in the wetwell, so that the drywell pressure remained essentially constant during the entire blowdown process. Although our system was not intended to be geometrically identical to any particular existing containment system, its gross geometrical parameters did roughly simulate the G.E. Mark 1 system (see Table 1).

Wetwells of three different sizes were tested, having diameters $D = 14$ cm, 28 cm, and 55 cm. These will be referred to as our small, medium-sized, and large wetwells, respectively. The height of the small and medium-sized systems was $2.18D$. In both, the wetwell was precisely half full of water, and the downcomer submergence was $0.364D$. The total height of the large system was $2.09D$, that is, it was slightly mis-scaled compared with the others. However, the downcomer submergence and the height of the airspace were exactly the same in the large system as in the small and medium-sized systems, although the depth of the water was $1.00D$ instead of $1.09D$. We believe that this difference is insignificant, because high-speed films have shown that, beneath the bubble

1776 234

which forms during blowdown, the water is essentially stagnant. The floor pressure is then transmitted across stagnant water, and should not be affected by small changes in the depth of the water. It is, however, important to properly scale the downcomer submergence and the height of the airspace, as was done.

The small and medium-sized wetwells were made of plexiglas, with side wall thicknesses of 0.6 cm and 1.3 cm, respectively. In both systems the roof and floor consisted of plexiglas plates about 2 cm thick. A second small wetwell, with precisely the same internal dimensions as the plexiglas one, was made out of 3 cm thick steel: this was our small system with absolutely rigid walls. The large system was PVC with a side wall thickness of 0.6 cm (heavily reinforced and braced) and roof and wall thicknesses of about 3 cm.

Blowdown was initiated in our system by a pneumatically operated valve consisting of a rubber-lined flat disc that pressed against the top of the downcomer when the valve was closed and which was rapidly withdrawn to open the valve. The opening time was short and did not affect the ensuing flow processes.

The test sections were instrumented to measure pressures (via Kistler Model 206 low-pressure piezotron transducers) at four locations (transducer numbers 1-4) as shown in Fig. 2. The response of the transducers was recorded on a storage oscilloscope and the traces were then photographed for subsequent analysis. High-speed films (1000 frames per second) were also taken of the pool swell in our

AES 2571

1776 235

small and medium-sized test systems.

The discharge coefficient associated with the gas flow rate through the downcomer could be independently controlled by placing interchangeable orifice plates in the downcomer, 11.5 downcomer diameters upstream of the downcomer exit (Fig. 2). The orifices were calibrated with each of the three gases that were used in our experiments. This calibration for C_m as a function of $(P_D - P)/P_D$ [where P is the pressure at the downcomer exit--see Eq. (4)] was performed by setting the drywell pressure at P_D and the wetwell pressure at $P_w = P$ and measuring the initial rate of pressure rise in the empty wetwell (containing no liquid) when the valve was opened. Using the first law of thermodynamics, and assuming adiabatic conditions, it is easy to show that

$$C_m = \frac{V}{\frac{\pi d^2}{4} \gamma \sqrt{2RT_D}} \left(\frac{P_D - P}{P_D} \right)^{\frac{1}{2}} \frac{1}{\tau} \quad , \quad (13)$$

where V is the total volume downstream of the orifice (wetwell plus downcomer) and τ is the time it would take the wetwell pressure to reach P_D if it were to keep rising at its initial rate. Figure 3 shows some typical results of orifice calibrations for different gases. The dependence of C_m on $(P_D - P)/P_D$ appears to be quite insensitive to the other parameters d_i/d , γ , and Re in Eq. (4), since the curves in Fig. 3 for different gases and different orifices have quite similar shapes. Thus modeling requirement (b) in the previous section was fully satisfied. We have chosen the value of C_m at $(P_D - P)/P_D = 1/3$ as a

1775 236

reference value for each gas-orifice combination, and it is that value which is used in comparing the experimental results discussed in the next section.

Our goal in these experiments was to test the scaling laws outlined in Section 2 by varying the quantities P_D , P_W , ρ , D , R , and C_m , which are the easily altered scaling parameters, and determining whether the dimensionless dependent variables, such as the dimensionless pressure, were functions of only the dimensionless groups, Eqs. (7)-(11).

In our test program, the linear system size was varied by about a factor of four: $D = 14-55$ cm.

Three gases were used: air (with $\gamma = 1.4$) and helium and argon (with $\gamma = 1.67$). The latter two were chosen because their gas constant R differs by a factor of 10, and hence allows the parameter π_4 [Eq. (11)] to be changed by a factor of 3.2 by changing gas alone, without changing pressures, flow orifice, or system size.

Two liquids were used: water and Meriam manometer fluid (1,1,2,2-tetrabromoethane, specific gravity 2.95). Flow constriction diameters relative to the downcomer diameter, d_i/d , were varied by a factor of 2. Absolute pressures were varied by a factor of about 6 in the wetwell and 9 in the drywell.

Table 2 shows the corresponding ranges over which the dimensionless scaling parameters were varied in our tests. Also shown for reference are the values of the same parameters for a design basis LOCA in a G.E. Mark 1 containment system.

1112 520

1776 237

TABLE 2. Values of Dynamic Scaling Parameters

<u>Parameter</u>	<u>Mark 1 System</u>	<u>Our System (Design Conditions)</u>
$\pi_1 = \gamma$	1.4	1.4, 1.67
$\pi_2 = P_w/\rho g D$	2 - 3 †	4.15, 8.29
$\pi_3 = P_D/P_w$	1 - 3	2.0, 3.0
$\pi_4 = C_m (RT_D/gD)^{1/2}$	c:a 25 †	8.5 - 6.0

† For the Mark 1 system, we take $D^2 \equiv \frac{4}{\pi} \times (\text{pool area per downcomer})$.

1776 238

P25 2511

4. RESULTS AND DISCUSSION

4.1 Typical Pressure Histories

Figure 4 shows some pressure traces measured in the medium-sized system ($D = 28$ cm). Trace 4(a) is the pressure on the wetwell floor, center (transducer #1, Fig. 2), trace 4(b) is the pressure on the wetwell ceiling (transducer #3), and trace 4(c) is the pressure in the downcomer just downstream of the orifice (transducer #4). The function of transducer #4 was to signal the initiation of blowdown, and we measured all times from the start of the increase in pressure of this transducer. Since that transducer was in communication with the downcomer via a narrow hole ($1/16$ " in diameter and several inches long), its response may have been partially attenuated by the intervening line. Thus trace 4(c) should not be used for inferring detailed quantitative information about conditions in the downcomer. The floor pressure measured off-center (transducer #2, Fig. 2) was virtually identical to the center floor pressure in our tests. The main features of the traces shown are typical of those obtained in all three systems, with all the gases tested. Figure 4(a) is a trace of the wetwell floor pressure which has a "clean" first peak with no superposed oscillations. Such oscillation-free floor pressure traces were obtained only when special precautions were taken to suppress small suspended gas bubbles in the pool, as will be discussed in more detail later. All the traces in Fig. 4 show the departure in pressure at a

given point from the initial pressure at that point before the initiation of blowdown: $P_1 - P_1(0)$, for example.

4.2 Verification of the Scaling Laws

To check for scaling we set out to verify whether the dimensionless forms of the pressures we measured were indeed functions only of the four modeling parameters π_1 to π_4 and the dimensionless time $t^* = t\sqrt{gD}$. Since our drywell pressure was constant, we found it convenient to define the dimensionless pressure as

$$p^* \equiv \frac{P - P(0)}{P_D}, \quad (14)$$

where P is the pressure at a given point and time, and $P(0)$ is the initial, pre-blowdown pressure at the same point. Our purpose is to show that

$$p^* = P^*(\pi_1, \pi_2, \pi_3, \pi_4, t^*), \quad (15)$$

but that P^* is not affected independently by any of the separate quantities that make up π_1 to π_4 and t^* . Rather than comparing the entire pressure histories for different cases, it is convenient to select some easily recognizable characteristics of the pressure histories and restrict the comparison to those. We have selected the following:

- (1) The first peak in the floor pressure, which occurs just

1776 240

1776 240

after vent clearing [Fig. 4(a)].

- (2) The time corresponding to the first peak in the floor pressure.
- (3) The minimum floor pressure after vent clearing [Fig. 4(a)].
- (4) The time corresponding to the minimum floor pressure after vent clearing [Fig. 4(a)].
- (5) The first peak in the ceiling pressure [Fig. 4(b)].
- (6) The time corresponding to the first peak in the ceiling pressure [Fig. 4(b)].

All of the five quantities listed above should be a function only of π_1 to π_4 .

We note first that our tests uncovered two effects which may cause deviations from the currently accepted scaling laws if the model scale is made too small. The first is caused by excessive water vapor in the wetwell airspace, and tends to give reduced peak uploads. For proper scaling, the absolute pressures must be reduced in proportion to system size, and consequently the proportion of water vapor in the wetwell airspace increases as the model size decreases. This tends to reduce the pressure rise due to the airspace compression, and hence the uploads. The effect can be significant at scales less than about 1/10 at room temperature, but we found that in our experiments the problem could be minimized by cooling the water to near freezing and thereby reducing its vapor pressure (see discussion in Section 4.3 below). All the ceiling pressure data shown from the small and medium-sized systems with water as the liquid are for pool temperatures not too far from freezing.

045 2511

1775 241

This precaution was not taken with the large system, however, where the absolute gas pressures were relatively high. Nor was it necessary to cool the smaller system when Meriam fluid was used as the wetwell liquid; that fluid has a very low vapor pressure even at room temperature.

The second effect is due to the presence of very small air bubbles suspended in the water or attached to the wetwell walls. These can give a "springiness" to the pool and can cause an effect similar to the fluid-structure interactions which might occur if the containment walls themselves were flexible, namely, an oscillatory component on the pressures measured in the wetwell pool. High-amplitude oscillations can be generated after the almost impulsive loading of the floor that occurs immediately after downcomer clearing. In the presence of the superposed oscillation, floor pressures are no longer properly scaled and the apparent peak downloads can be considerably higher than one would get in the absence of bubbles. The air bubble problem can be eliminated, however, by the addition of a surfactant (such as Kodak "Photo-Flo") to the wetwell water, or by using a different wetwell liquid (such as Meriam manometer fluid) (see discussion in Section 4.4 below). Under these conditions, measured downloads scale according to the Moody laws. All the data we show on the scaling of the first peak in the floor pressure (which occurs in response to the almost impulsive loading following vent clearing), with water as the wetwell liquid, are taken with Photo-Flo added. In the experiments in the small system with Meriam fluid as the wetwell liquid, there appeared to be no problems with bubbles.

1776 242

Figure 5-14 summarize our results on scaling from all the air tests with both water and Meriam fluid as the wetwell liquids. Note that not all of the graphs include data from all three systems. Figures 5 to 11 plot dimensionless pressures $P_1 - P(0)$ against π_4 with π_1 , π_2 , and π_3 held constant; Figs. 11 to 14 plot dimensionless times $t\sqrt{g/D}$ against π_4 , again with π_1 to π_3 held constant. Results for tests at two values of π_2 ($\pi_2 = 4.15$ and $\pi_2 = 8.29$) and at two values of π_3 ($\pi_3 = 2$ and $\pi_3 = 3$) are shown. The time marked "vent clearing" is actually the time measured for the first peak in the floor pressure, which occurs just after vent clearing.

The results constitute clear support for the scaling laws. Allowing for some scatter in the data, the dimensionless dependent variables appear to be functions of only the proposed scaling parameters. At the same values of π_1 to π_4 the tests in systems of different size (differing in linear dimension by up to a factor of 4) have the same dimensionless pressures or times. It should be emphasized that the dimensional dependent variables--for example, the raw pressure data that appear in dimensionless form in Fig. 9--differ in magnitude by up to 400%. Only when reduced to dimensionless form do the data for each variable fall on a single smooth curve as shown.

Figures 15 to 24 are results from the helium and argon tests in the three wetwells. Again, dimensional pressures and times have been plotted against π_4 . In view of the wide range of three of the experimental parameters varied in these tests--a factor of 10 in gas enthalpy, 3 in liquid density, and 4 in system size--the agreement in the dimensionless

SAS 2111

1776 243

dependent variables is very good. The importance of the gas enthalpy, which appears in π_4 , is clearly confirmed: dynamically similar tests with helium and argon in the same wetwell system required different downcomer orifices, such that the π_4 's were matched, to give satisfactory agreement in the recorded pressures and times.

The central role of the enthalpy flux parameter π_4 in modeling the pool swell can be further emphasized by comparing data from systems that have the same values of π_1 to π_3 , but have geometrically similar orifices (i.e., are completely geometrically similar) instead of having the same values of π_4 . Figure 25 shows the data from Fig. 9 for the air/water tests in the three systems, but the ordinate is now d_i/d (a dimensionless orifice diameter) which is an indication of downcomer geometry, rather than of π_4 , the measured enthalpy flux. It is clear that with π_1 to π_3 exactly matched in the three systems, and at the same value of d_i/d (i.e., exact geometric similarity), but with different π_4 , the dimensionless pressures measured in the three systems are quite different. The point can be made even more strongly by replotting the data from the helium and argon tests. Figures 26 and 27 show the same data as Fig. 19, plotted against the new ordinate d_i/d . The behavior of the two gases and of the different size systems now appears vastly different. The conclusion is that proper orificing of the downcomer line is an important ingredient of the scaling procedure.

1776 244

205 2551

4.3 Effect of Excessive Vapor Pressure in Small-Scale Tests

Our initial test series showed that in experiments with water at room temperature in the wetwell the dimensionless ceiling pressures in the small system ($D = 14$ cm) fell below the corresponding values in the medium-sized system ($D = 28$ cm), and these in turn fell somewhat below the values in the large system ($D = 55$ cm). However, in tests conducted at low wetwell pool temperatures (close to freezing), dimensionless histories in all three systems with water were the same and agreed with the results from tests in the small system with Meriam fluid. We attribute this behavior to the presence of water vapor in the wetwell airspace prior to blowdown in the higher temperature tests. Significant amounts of water vapor will not only change the value of γ for the gas in this region, but may also provide a mechanism for condensation and rapid heat transfer during pool swell. These effects are, of course, not accounted for in the scaling analysis. At room temperature the vapor pressure of water is about 3 kPa--a significant fraction of the initial wetwell pressure, 5.67 kPa, required in many of the small system tests. By cooling the wetwell pool in an ice-water bath the water vapor pressure is reduced to about 0.5 kPa, a value which is apparently low enough not to affect the compression of the wetwell airspace significantly.

After we identified this problem, we conducted tests with the small and medium-sized systems in ice-baths, so that the water was just slightly above freezing. Figures 28 to 30 show the effects of changing the temperature. The solid points represent data taken for water at room

temperature. The open points represent data taken when the vapor pressure was negligible--for the small and medium-sized systems an ice bath, and for the small system with Meriam manometer fluid. The curves on the plots are drawn through the low vapor pressure data and the data from the large system. Note that for fixed values of π_1 , π_2 , and π_3 , the points from the small system are in general below those of the medium-sized system. This is because the small system is operating at lower absolute pressures. Similarly, there is less deviation as π_2 is increased.

Tests in the large system have not yet been conducted in an ice bath. It appears from our figures that there might be some slight effect even in this system. In experiments with Meriam manometer fluid (specific gravity 2.95) replacing water as the wetwell liquid, we have found the vapor pressure effect to be entirely absent--a result consistent with the extremely low vapor pressure of this liquid at room temperature (about 0.003 kPa).

Tests of the floor pressure in our medium-sized system have shown no vapor-pressure effects, and we believe this to be true of our small system also. All of our floor pressure data, with or without surfactant, was taken at room temperature. Generally, in tests with helium, the water vapor problem appeared to be most acute. We attribute this to the fact that helium equilibrates more quickly with water than either argon or air.

It is not surprising that the first indication of conditions in which there is a departure from the scaling laws came from the tests

in our smallest system. Apart from the rigidity of the walls and the incompressibility of the liquid, the key assumptions underlying the development of the modeling laws in Section 2 are: perfect and noncondensable gases in the drywell and wetwell, negligible heat transfer from gas to liquid, inviscid motion in the wetwell pool, and negligible surface tension effects. All of these assumptions are more likely to be satisfied as system size is increased. Our results show that except for the first assumption (noncondensable gas in the wetwell pool), the assumptions do hold in systems as small as our smallest wetwell ($D = 14$ cm), and that provided the pool is cold, even the first assumption is satisfied. This conclusion is very encouraging. The scaling laws clearly do hold in the small-scale systems that we have tested, going down to about 1/24 of full-scale Mark 1 conditions, and there is every reason to believe that they will be equally applicable in any larger-scale tests.

4.4 On the Precautions That Must be Taken to Avoid Pool Oscillations due to Gas in the Liquid

As we noted above, most of our original tests with water as the wetwell liquid showed a strong oscillatory component superposed on the floor pressure near the time of vent clearing (Fig. 31b). The oscillatory component appeared to have been caused by pool oscillations which resulted from the presence of air in the liquid, presumably in the form of very small bubbles either in the liquid or at the liquid/solid boundaries. That the bubbles were the cause, and not actual wall flexure

0AS 2511

1775 247

and oscillations (true fluid-structure interactions), was deduced from three observations. First, tests in the absolutely rigid-wall small system, which had 3 cm thick steel walls, showed floor pressure oscillations similar to those in the small system with plexiglas walls. Secondly, the addition of a surfactant (Kodak Photo-Flo, in an amount recommended by the manufacturer) removed the oscillatory component. Finally, when Meriam fluid was used as the wetwell liquid (in the small system only), there appeared to be no problem with trapped gas and the concomitant pressure oscillation.

The hypothesis that the pressure oscillations are due to pool vibrations which result from bubbles is further supported by Fig. 31, which shows a series of runs made with a light oil as the liquid (specific gravity 0.876). Runs were made every minute, and we show pressure traces of every other run. Figure 31a shows the first, smooth pressure trace obtained. Note that the first peak in the floor pressure is somewhat less than the final pressure. Figure 31b shows a trace obtained two minutes later--its appearance is similar to that of the water traces to which no surfactant has been added. The next three traces show the oscillations becoming progressively larger and larger. The maximum pressure in the last trace is almost four times that of the first (note the change in scale). We believe this sequence of traces obtained in rapid, consecutive blowdowns is explained by the progressive accumulation of bubbles suspended in the relatively viscous oil of the pool. Our hypothesis that the oscillations are due to bubbles is given further support by the fact that a trace taken

after the bubbles had had time to clear (e.g., by allowing the system to stand undisturbed, overnight) often had a shape free of superposed oscillations.

The scaling laws outlined in Section 2 do not, of course, account for the presence of bubbles and bubble-induced pool oscillations, and thus the peak floor pressures measured in tests performed without the appropriate precautions are not expected to obey scaling laws. It should be emphasized, however, that since the amplitudes of the pool oscillations were very small compared with system size, the bulk pool displacements, pool swell velocities, and pressures in the wetwell and downcomer airspaces were not significantly affected by the brief pool oscillations after vent clearing.

1776 249

BAS 2777

5. CONCLUSIONS

(1) Our experiments confirm the modeling laws outlined in Eqs. (7)-(12) for the air clearing phase of the flow into a water-type pressure suppression system. These are in essence the laws that were originally put forward by Moody,³ and they require that the enthalpy flux from the downcomer be scaled down in a small model by the use of an orifice, so that the scaling parameter π_4 is properly simulated. If this is not done (for example, as when an appropriate orifice is not used in the small-scale model, although the dynamic conditions are otherwise properly scaled), the wetwell pressures can be significantly mis-scaled. (One notes, however, that the first peak in the floor pressure, as well as all the characteristic times, were insensitive to π_4 in our tests, except near the very lowest values of π_4 that we tested.) With these laws, accurate small-scale testing of the process is possible.

(2) In order to ensure proper scaling in small-scale tests, it is necessary to take precautions against excessive vapor content in the wetwell "airspace." In tests with room-temperature water at sufficiently small scales (smaller than about 1:10 if the full-scale wetwell is at about standard atmospheric pressure) the presence of excessive water vapor in the wetwell tends to give reduced peak ceiling pressures. This effect of vapor pressure can, however, be minimized by cooling the water to a temperature near freezing, or by replacing the water with another liquid, such as Meriam manometer fluid, which

has a very low vapor pressure.

(3) Peak downloads on the wetwell floor can be expected to scale with the proposed scaling laws only if the containment walls are rigid and if precautions are taken to eliminate the presence of small air bubbles in the pool liquid. Both fluid-structure interactions caused by the flexure of the pool bounding walls, and the presence of air in the liquid, tend to give a "springiness" to the wetwell pool, and can cause high-amplitude oscillations in the floor pressure after the almost impulsive loading of the floor immediately after downcomer clearing. Such oscillations are not accounted for in the present scaling laws. One may expect that generally, the problem with air bubbles tends to get worse as scale is reduced. We note, however, that since the amplitudes of the oscillatory pool motion are very small when compared with system size, bulk pool displacements, pool swell velocities, and pressures in the airspaces are not affected by such pool oscillations. The problem with air bubbles can be eliminated by the addition of a surfactant (such as Kodak Photo-flow) to the wetwell water, or by using a particular wetwell liquid (such as Meriam manometer fluid) where the problem with bubbles appears not to arise. When these precautions are taken, and when the pool boundaries are rigid (that is, the period of their natural oscillation is much shorter than the shortest transient time in the imposed hydrodynamic loading), floor loads scale according to the proposed laws.

REFERENCES

1. Cudlin, R. and Kudrick, J.A., "Recent Considerations of Hydrodynamic Forces in Pressure-Suppression Containments (U.S.A.)," paper presented at the International Atomic Energy Agency Meeting on Thermal Hydraulic Consequences of LOCA's Inside and Outside Containments, Cologne, FRG, 7-8 December 1976.
2. Telford, J.T., "Current Problems in Reactor Safety," in Nuclear Power Safety (J.H. Rust and L.E. Weaver, Eds.), Pergamon Press, New York, 1976, pp. 351-358.
3. Moody, F.J., "A Systematic Procedure for Scale-Modeling Problems in Unsteady Fluid Mechanics," General Electric Company unpublished report, 1976.
4. Anderson, W.G., Huber, P.W., and Sonin, A.A., "Small-Scale Modeling of Hydrodynamic Forces in Pressure Suppression Systems: Tests of the Scaling Laws," paper presented at American Nuclear Society Meeting on Thermal Reactor Safety, July 31-August 4, 1977, Sun Valley, Idaho.

1776 252

825 2551

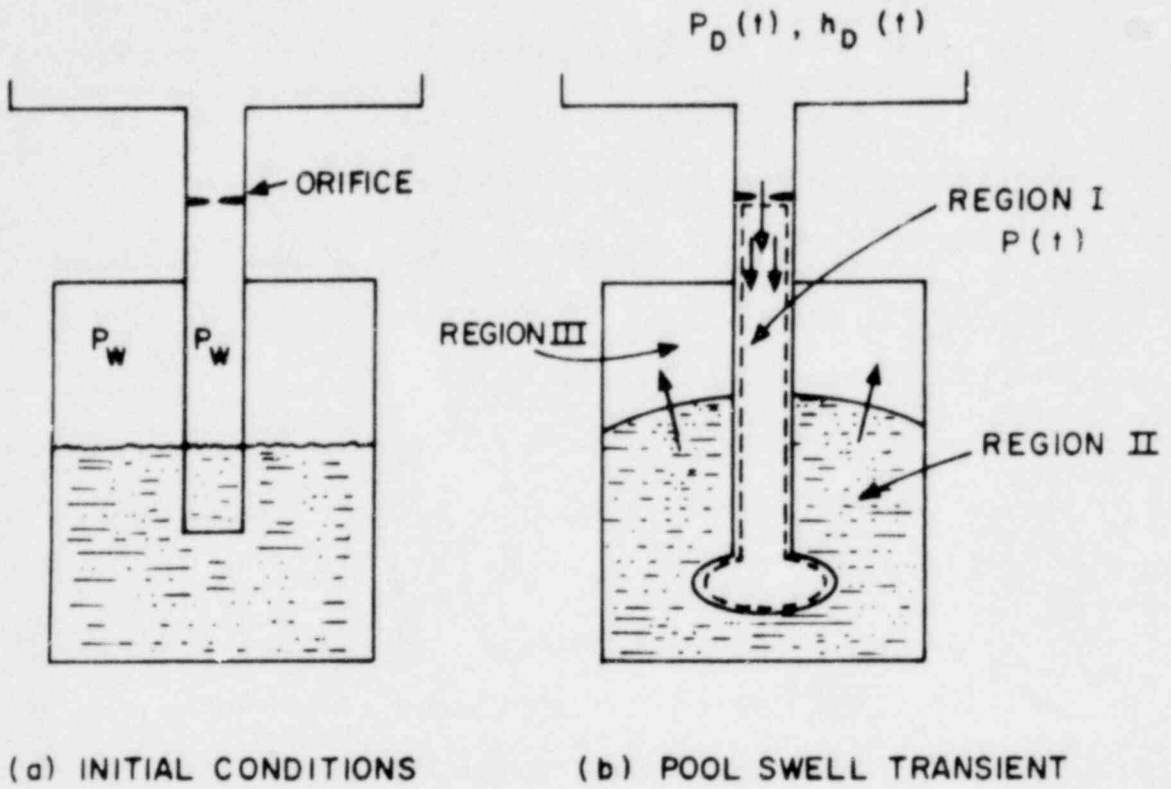


FIGURE 1. Modeling of pool swell for scaling laws.

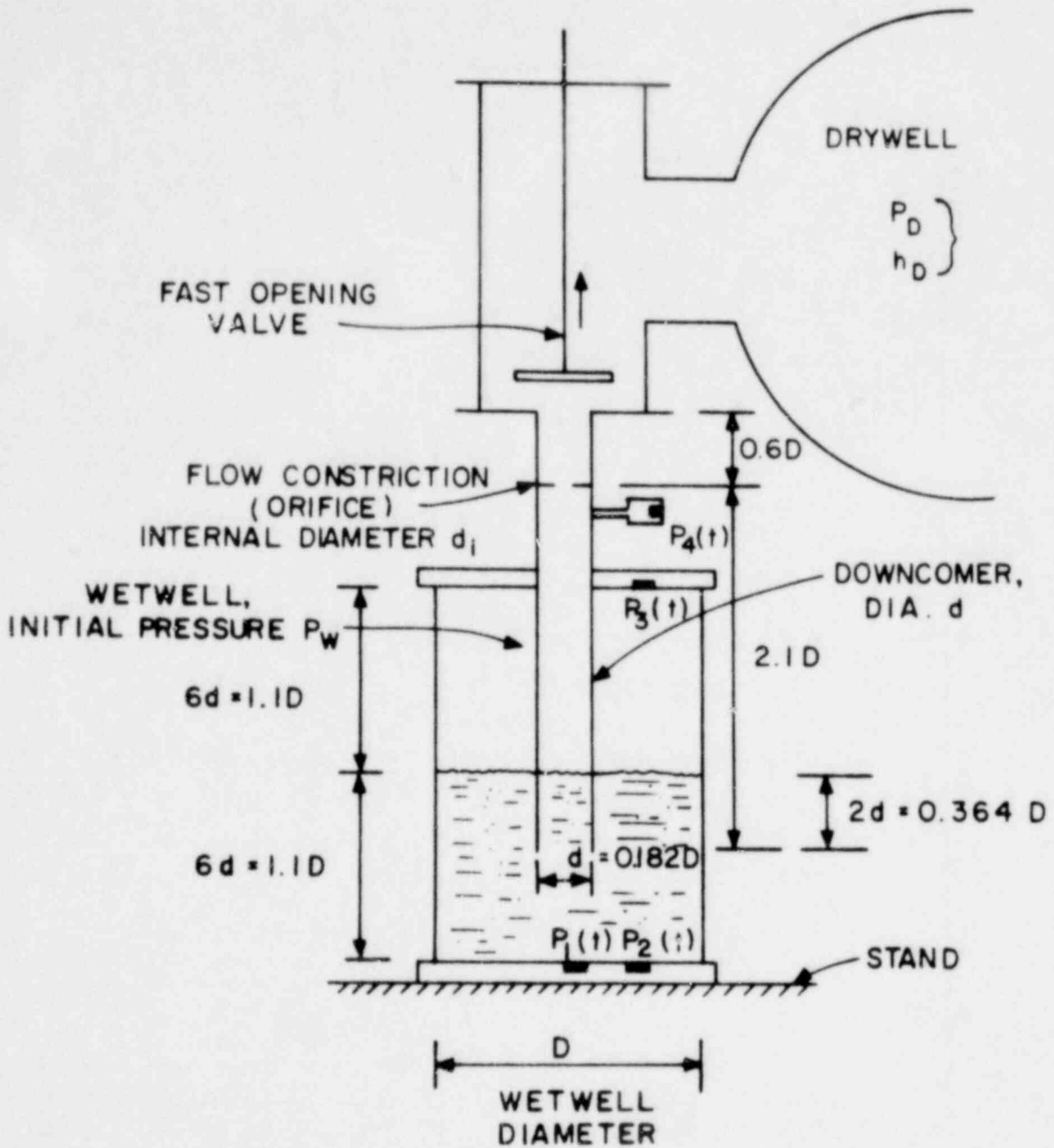


FIGURE 2. Experimental system.

1776 254

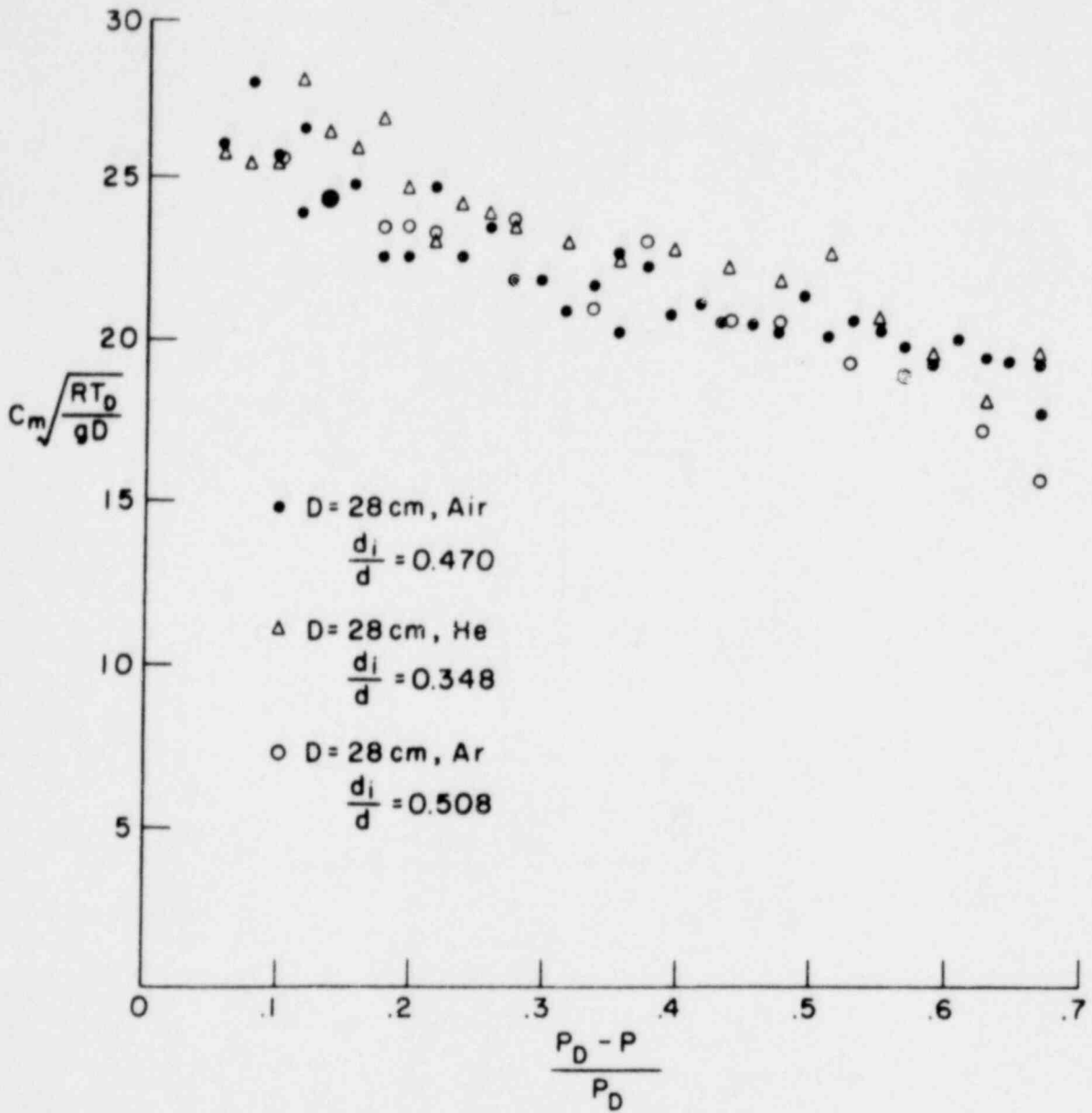


FIGURE 3. Typical orifice calibrations.

425 2551

1776 255

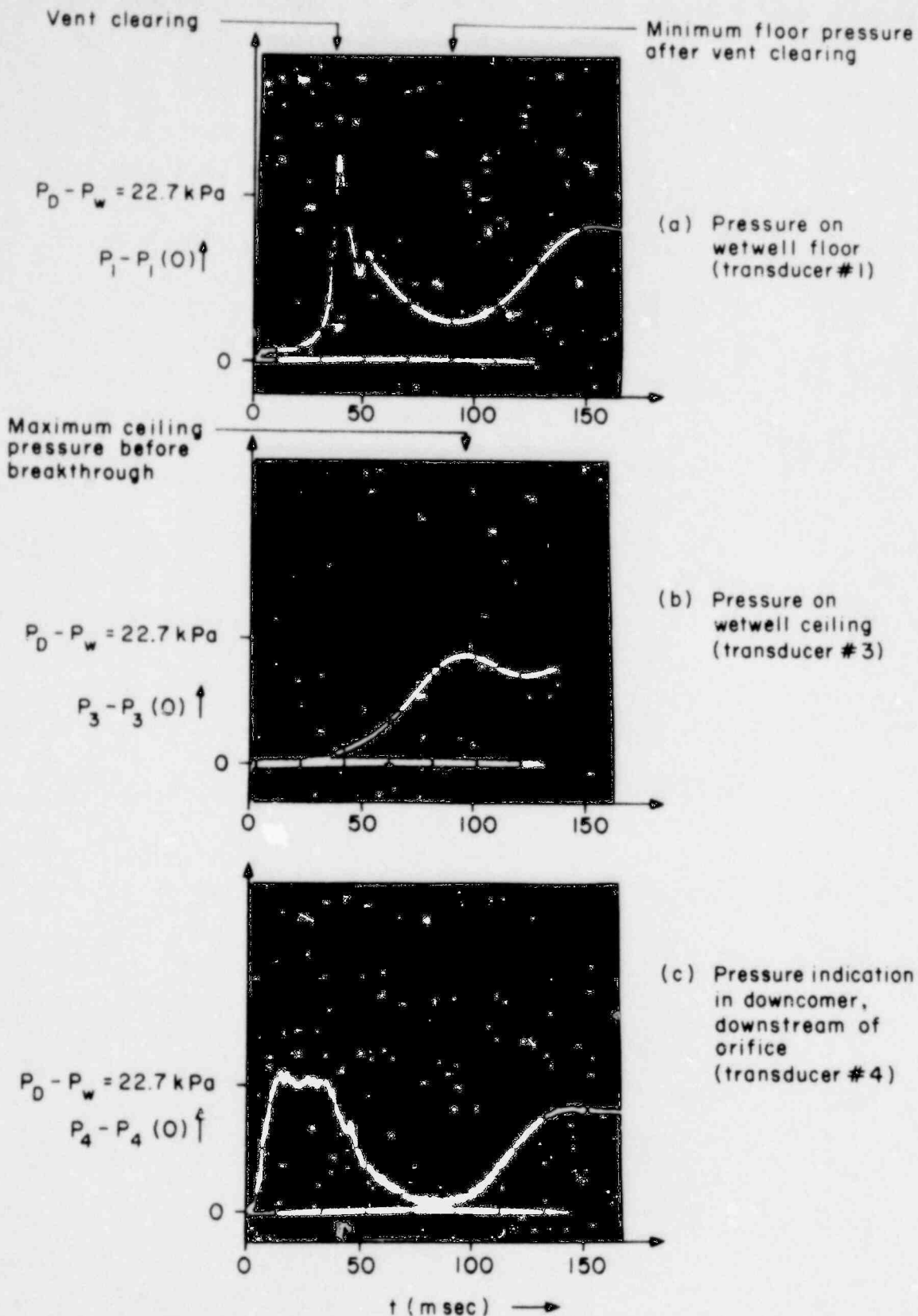


FIGURE 4. Pressure histories (air/water, $D = 28 \text{ cm}$, $\pi_1 = 1.4$, $\pi_2 = 4.15$, $\pi_3 = 3$, $\pi_4 = 21.4$).

1776 256

1776 256

$$\gamma = 1.4 \quad \frac{P_w}{\rho g D} = 4.15 \quad \frac{P_D}{P_w} = 2$$

Air	Liquid	D(cm)	P_w (Nm ⁻²)
□	Water	28	11,300
△	Meriam	14	16,700

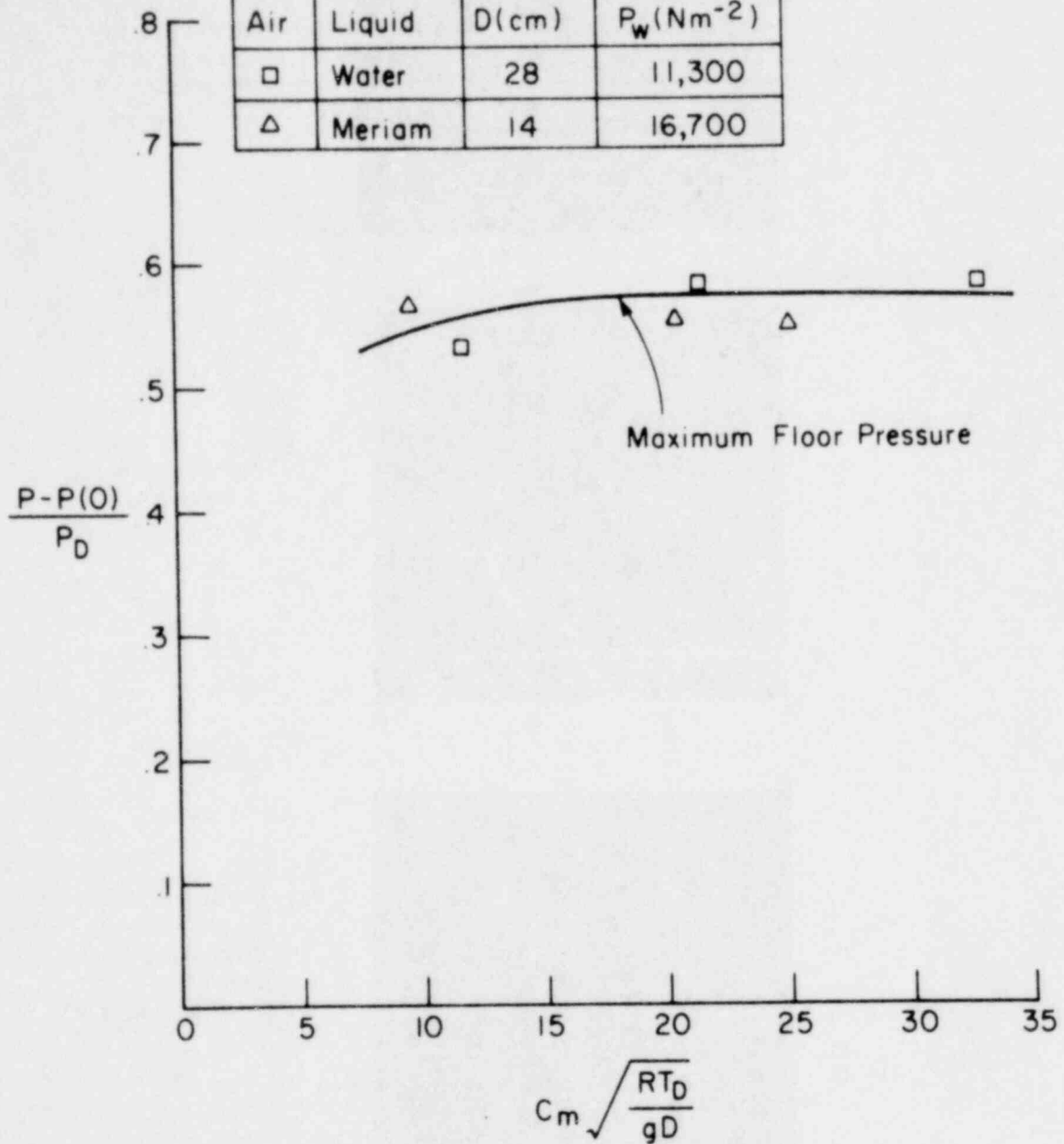


FIGURE 5. First peak in floor pressure versus π_4 .

1572 257

1775 257

$$\gamma = 1.4 \quad \frac{P_w}{\rho g D} = 4.15 \quad \frac{P_D}{P_w} = 3$$

Air	Liquid	D(cm)	$P_w(Nm^{-2})$
□	Water	28	11,300
△	Meriam	14	16,700

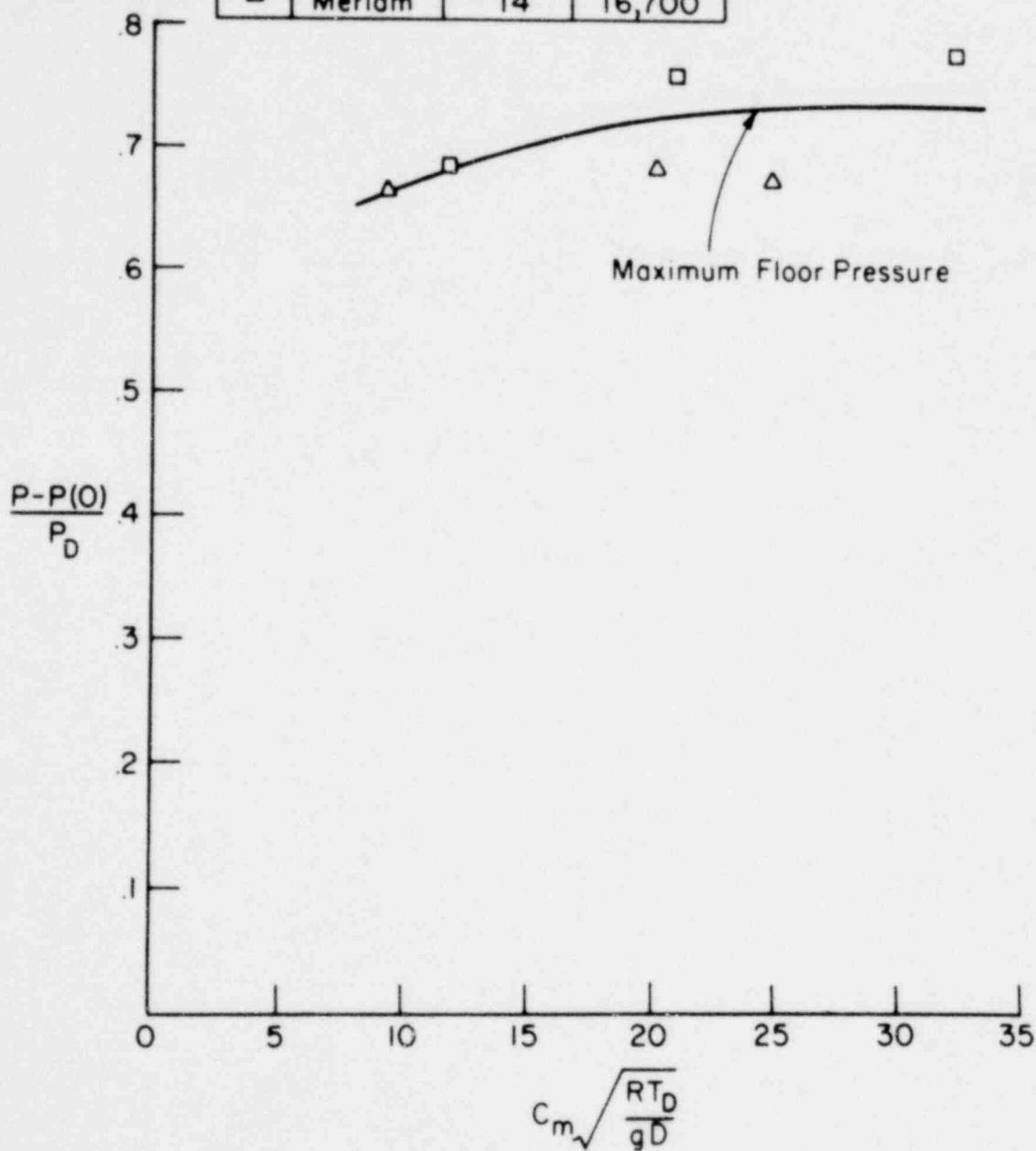


FIGURE 6. First peak in floor pressure versus π_4 .

1112524

1776 258

$$\gamma = 1.4 \quad \frac{P_w}{\rho g D} = 8.29 \quad \frac{P_D}{P_w} = 3$$

Air	Liquid	D(cm)	P_w (Nm ⁻²)
□	Water	28	22,700
△	Meriam	14	33,300

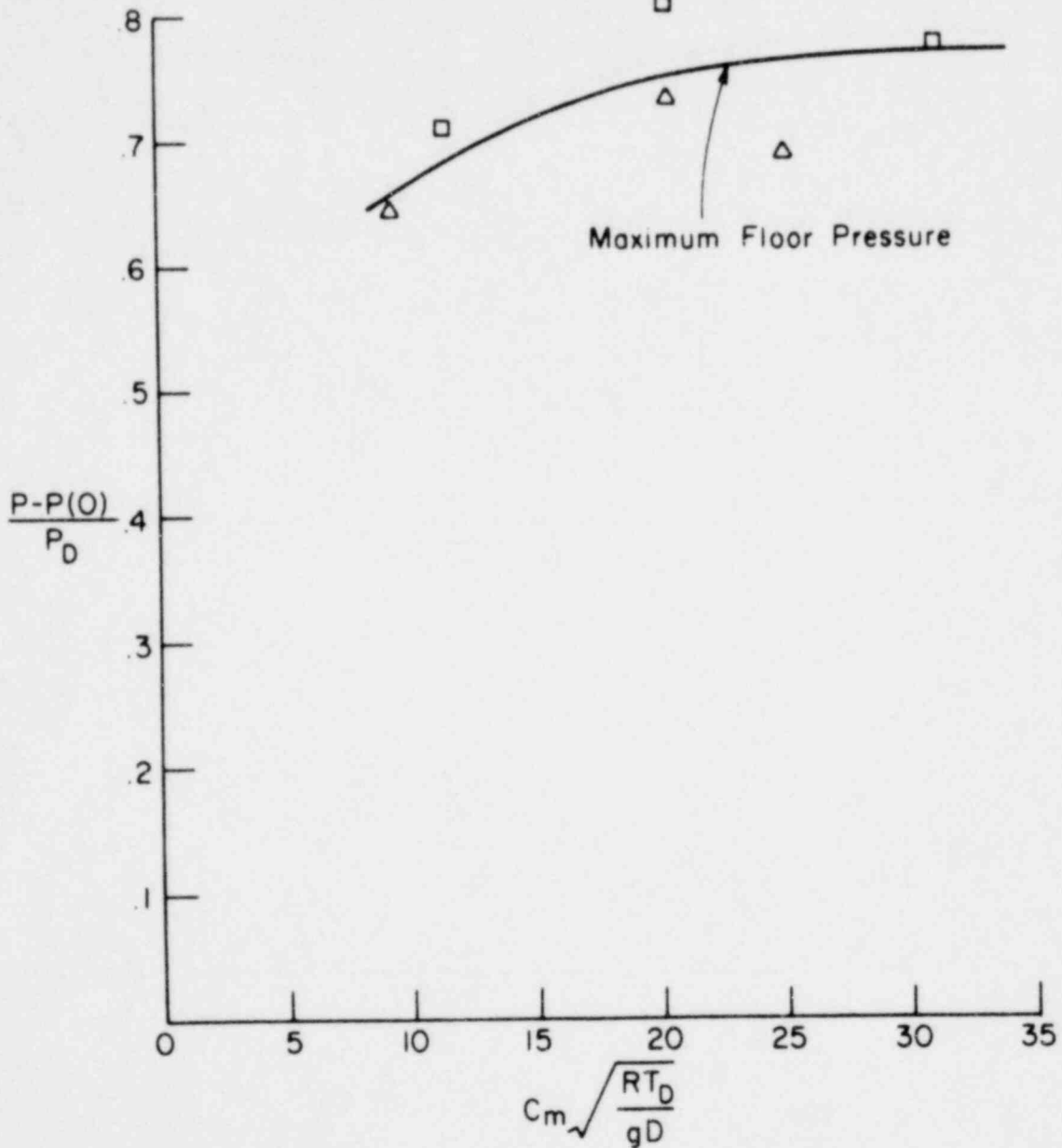


FIGURE 7. First peak in floor pressure versus π_4 .

825 2571

1776 259

$$\gamma = 1.4 \quad \frac{P_w}{\rho g D} = 4.15 \quad \frac{P_D}{P_w} = 2$$

Air	Liquid	D(cm)	P _w (Nm ⁻²)
○	Water (Ice Bath)	14	5,670
□	Water (Ice Bath)	28	11,300
▽	Water (Room Temp)	55	22,100
△	Meriam (Room Temp)	14	16,700

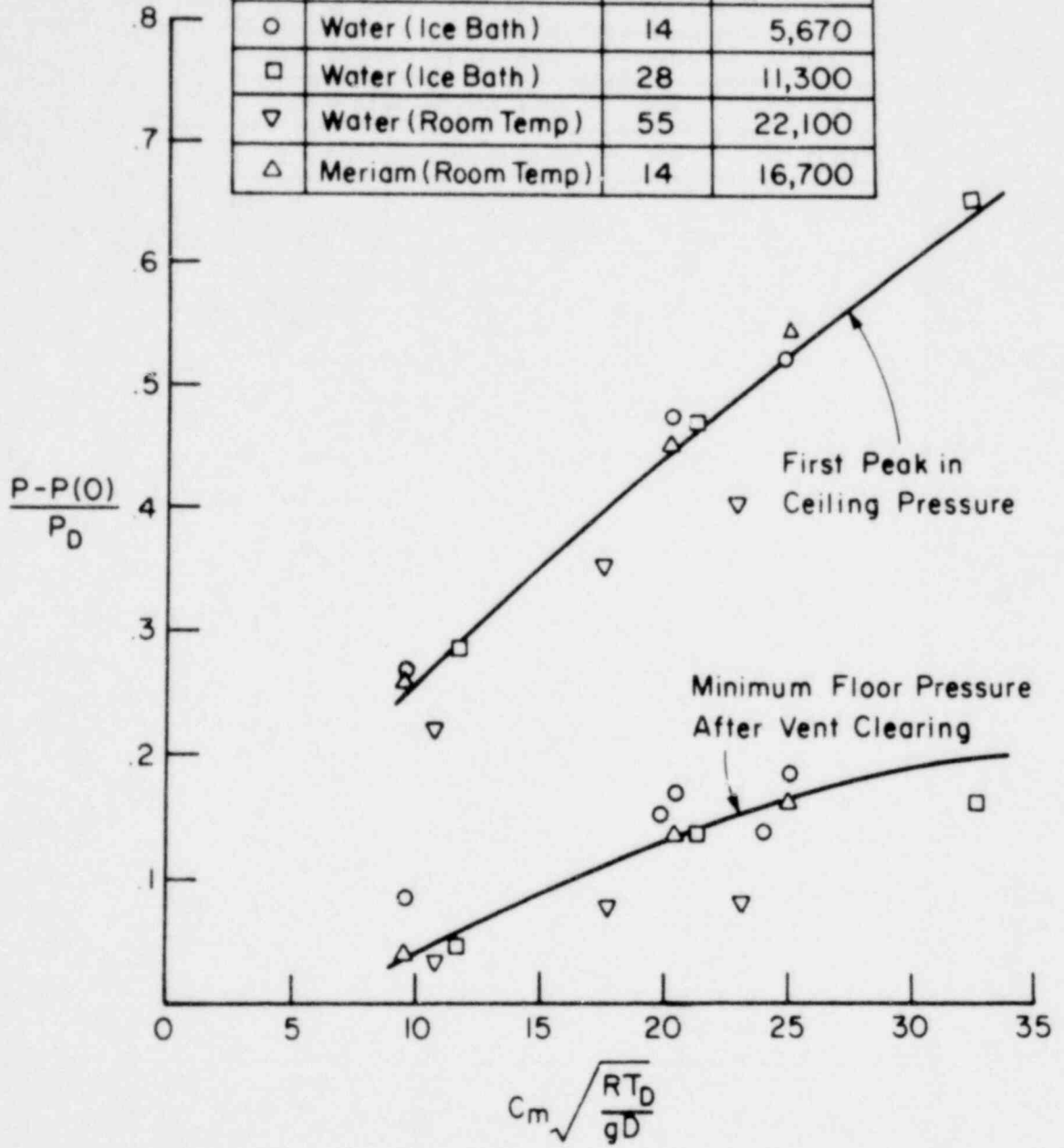


FIGURE 8. First peak in wetwell ceiling pressure and minimum floor pressure as functions of π_v .

1776 260

1185 2511

$$\gamma = 1.4 \quad \frac{P_w}{\rho g D} = 4.15 \quad \frac{P_D}{P_w} = 3$$

Air	Liquid	D(cm)	P_w (Nm ⁻²)
○	Water (Ice Bath)	14	5,670
□	Water (Ice Bath)	28	11,300
▽	Water (Room Temp)	55	22,100
△	Meriam (Room Temp)	14	16,700

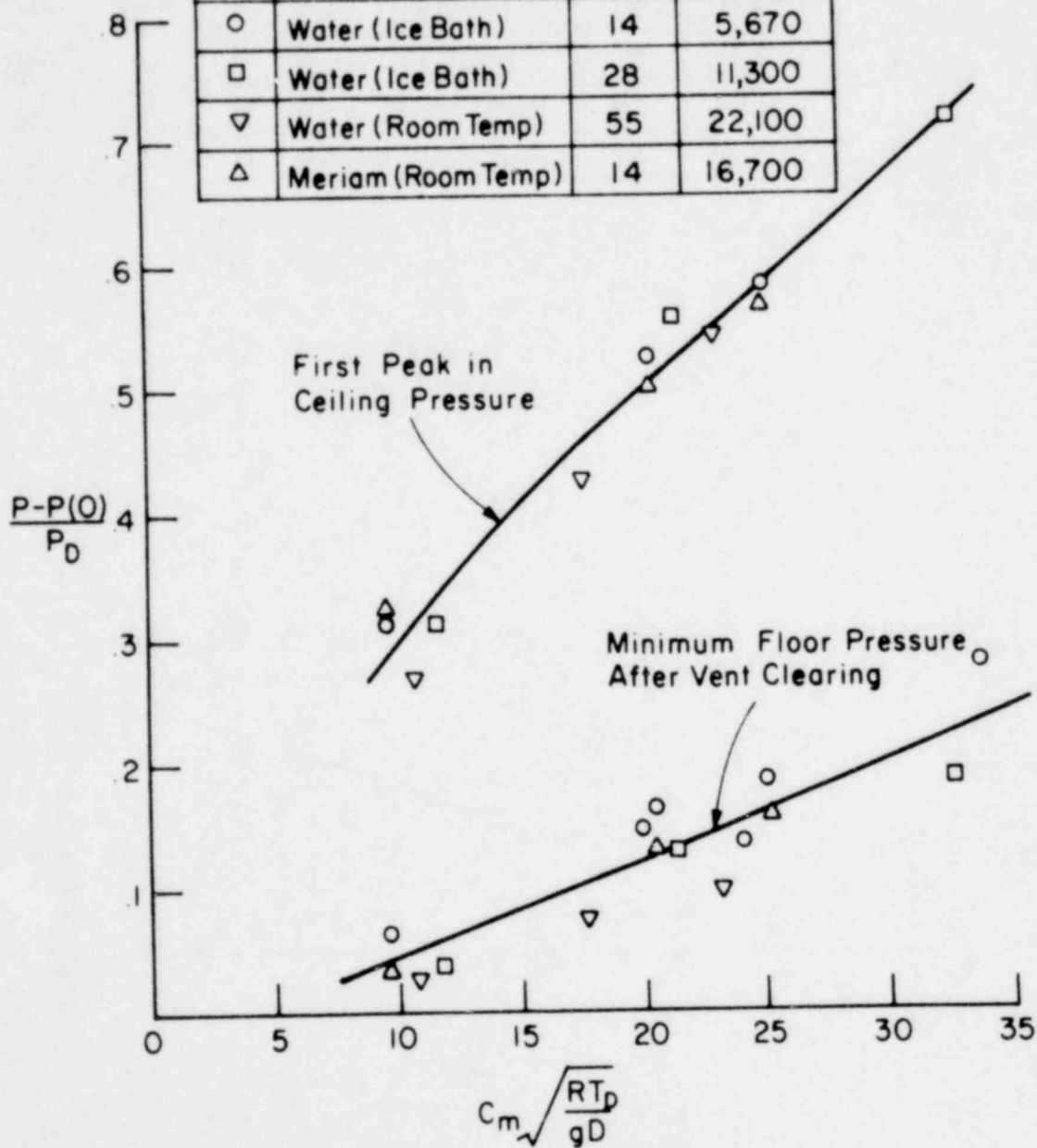


FIGURE 9. First peak in wetwell ceiling pressure and minimum floor pressure as functions of π_4 .

085 2511

1775 261

$$\gamma=1.4 \quad \frac{P_w}{\rho g D} = 8.29 \quad \frac{P_D}{P_w} = 3$$

Air	Liquid	D(cm)	$P_w(Nm^{-2})$
○	Water (Ice Bath)	14	11,300
□	Water (Ice Bath)	28	22,700
△	Meriam (Room Temp)	14	33,300

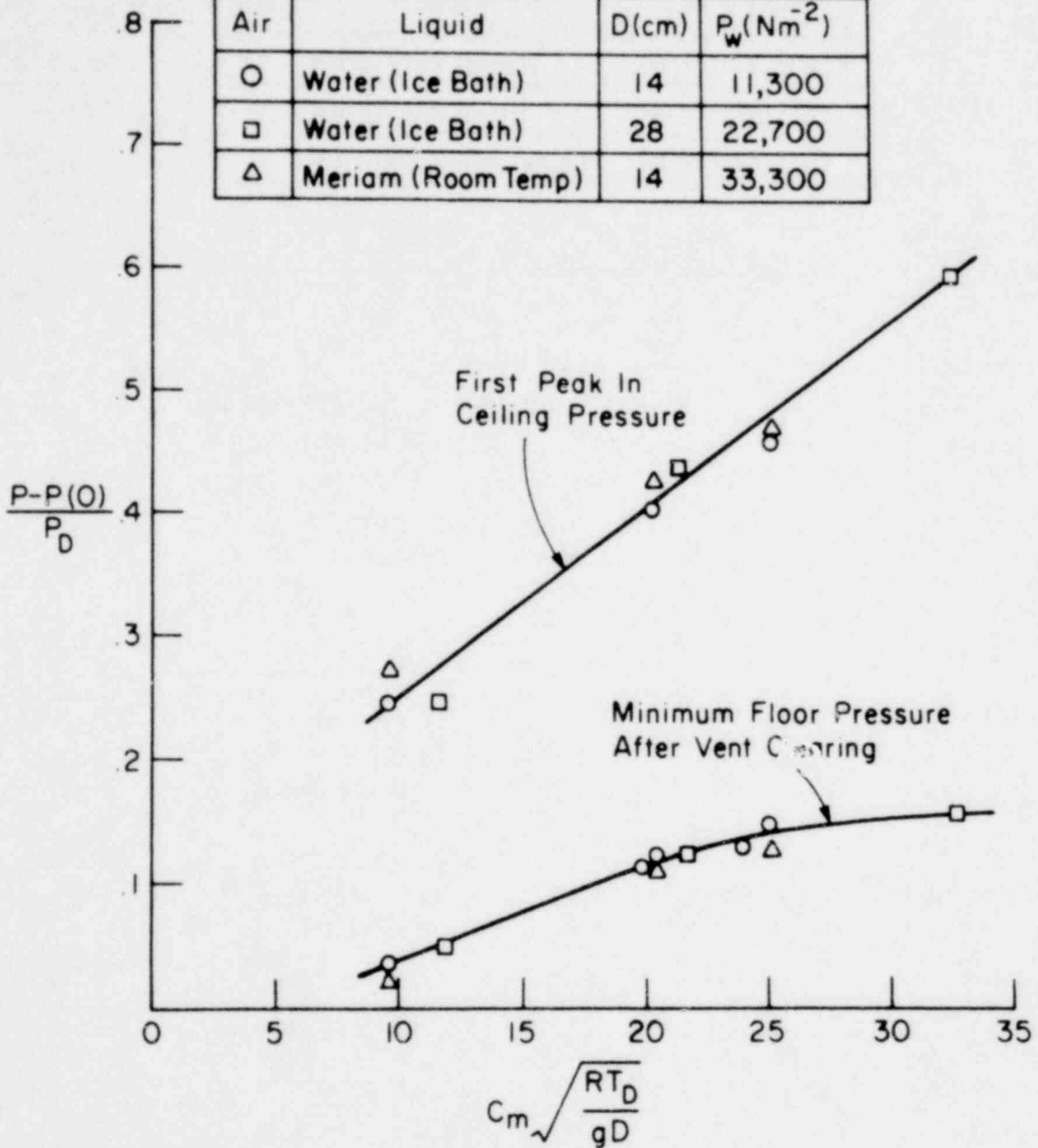


FIGURE 10. First peak in wetwell ceiling pressure and minimum floor pressure as functions of π_w .

1776 262

$$\gamma = 1.4 \quad \frac{F_w}{\rho g D} = 4.15 \quad \frac{P_D}{P_w} = 2$$

Air	Liquid	D(cm)	P_w (Nm ⁻²)
○	Water	14	5,670
□	Water	28	11,300
▽	Water	55	22,100
△	Meriam	14	16,700

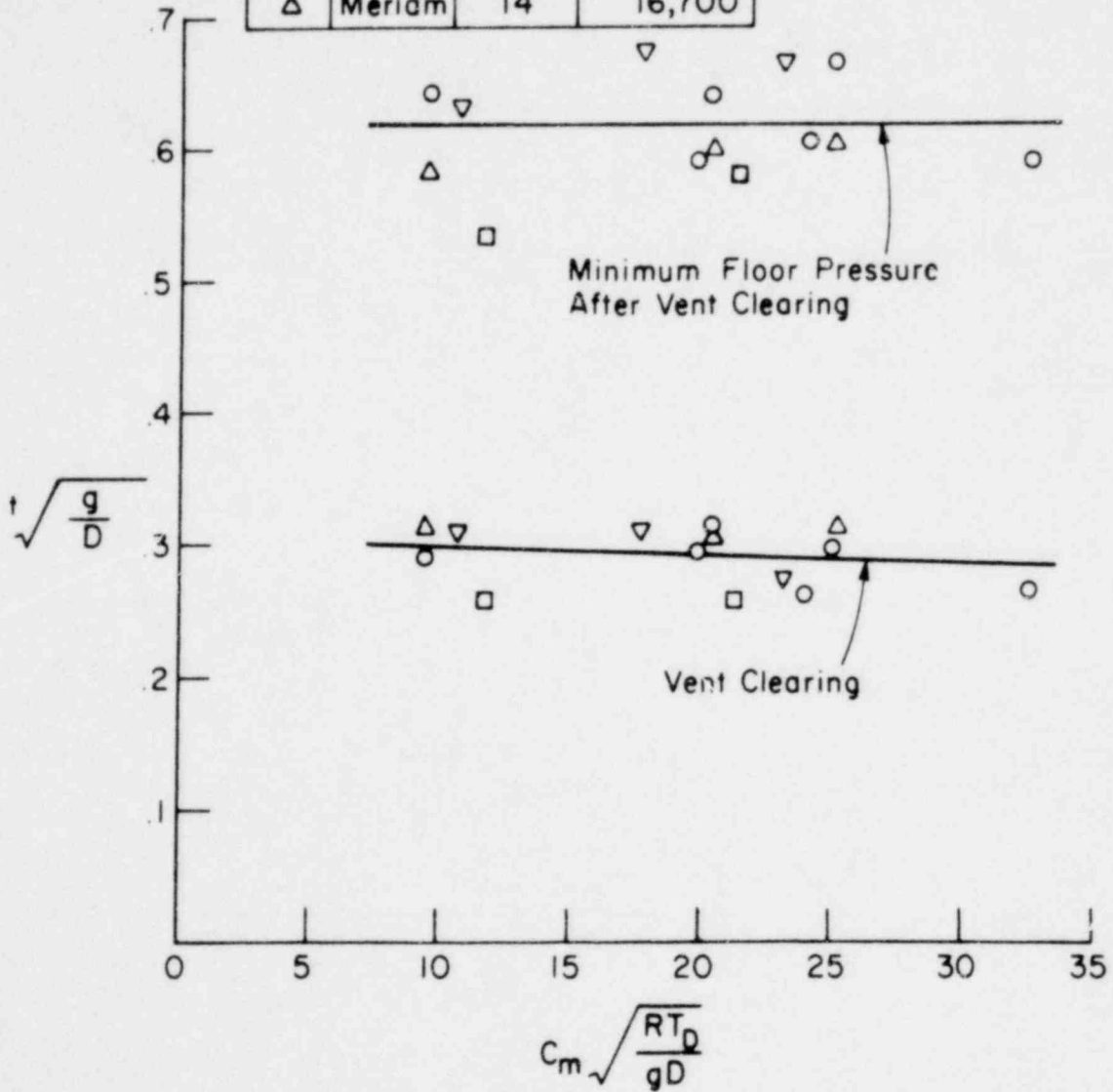


FIGURE 11. Dimensionless times versus π_4 .

1776 263

$$\gamma = 1.4 \quad \frac{P_w}{\rho g D} = 4.15 \quad \frac{P_D}{P_w} = 2$$

Air	Liquid	D(cm)	P_w (Nm ⁻²)
○	Water	14	5,670
□	Water	28	11,300
▽	Water	55	22,100
△	Meriam	14	16,700

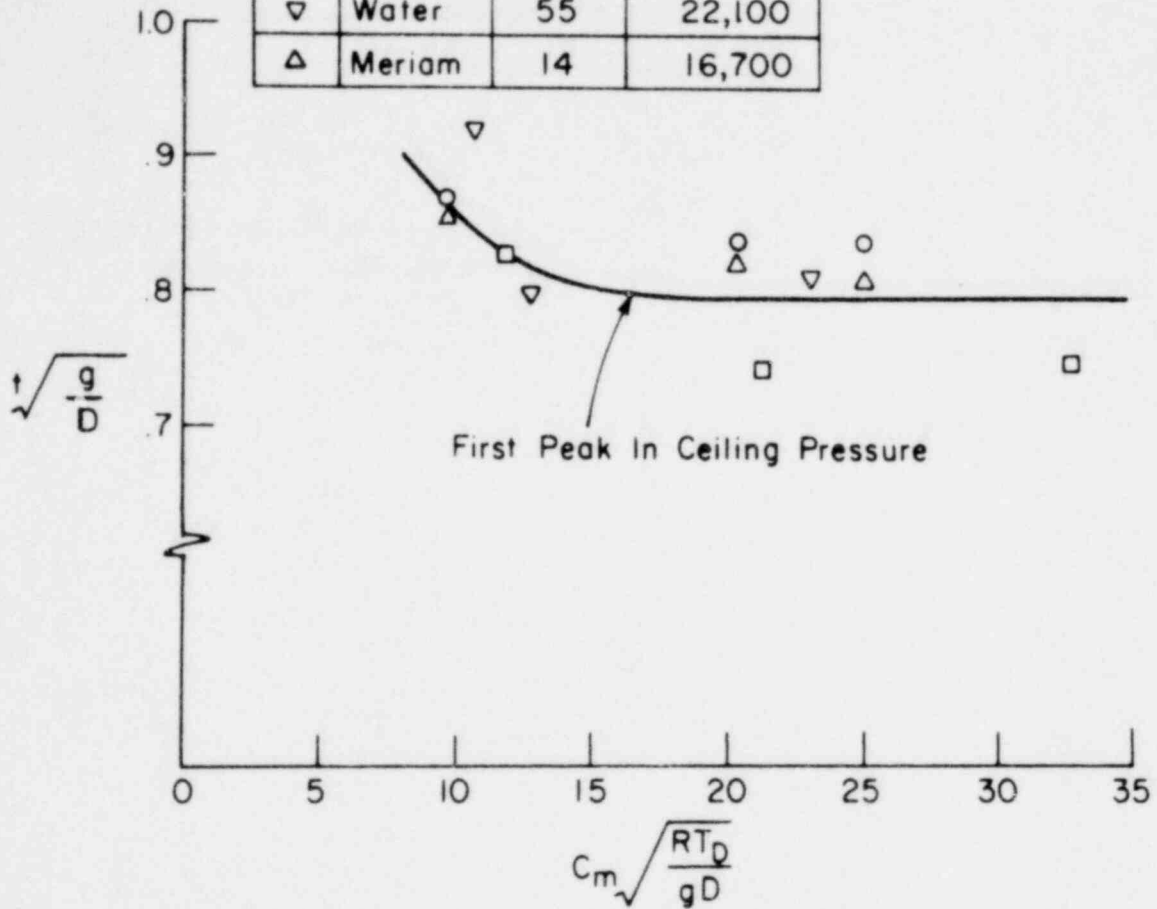


FIGURE 12. Dimensionless time versus π_4 .

1776 264

$$\gamma = 1.4 \quad \frac{P_w}{\rho g D} = 4.15 \quad \frac{P_D}{P_w} = 3$$

Air	Liquid	D(cm)	$P_w(Nm^{-2})$
○	Water	14	5,670
□	Water	28	11,300
▽	Water	55	22,100
△	Meriam	14	16,700

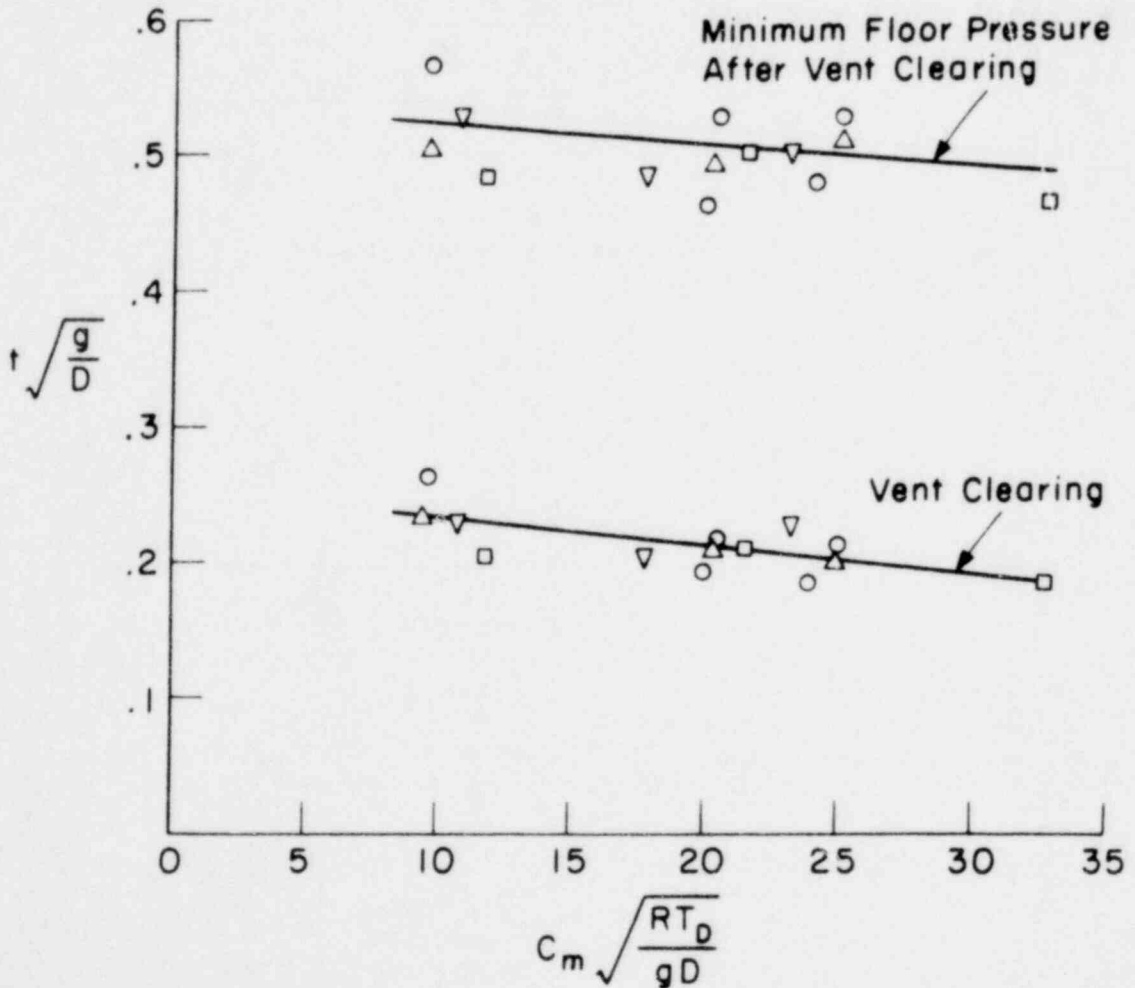
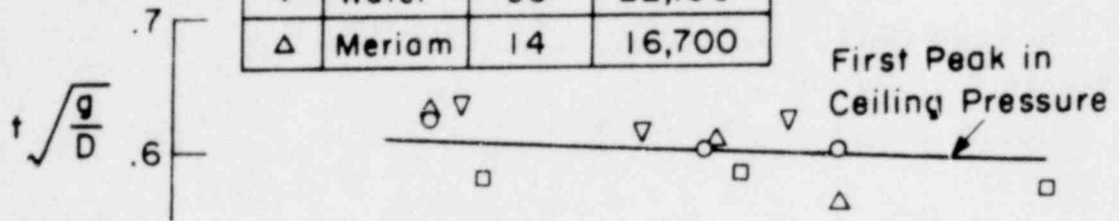


FIGURE 13. Dimensionless times versus π_4 .

1175 264

1776 265

$$\gamma = 1.4 \quad \frac{P_w}{\rho g D} = 8.29 \quad \frac{P_D}{P_w} = 3$$

Air	Liquid	D (cm)	P_w (Nm ⁻²)
○	Water	14	11,300
□	Water	28	22,700
△	Meriam	14	33,300

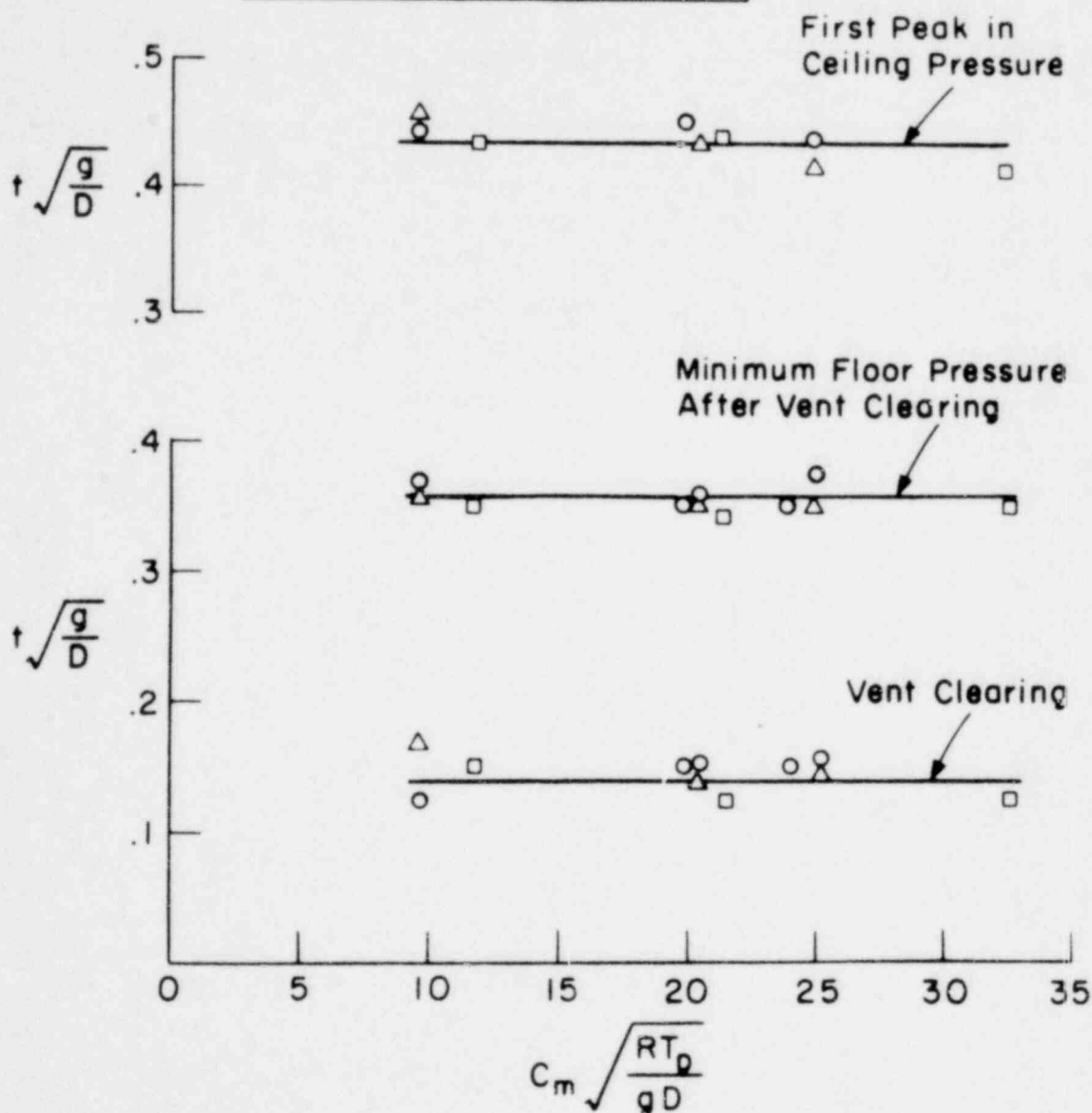


FIGURE 14. Dimensionless times versus π_4 .

1775 266

105 2551

$$\gamma = 1.67 \quad \frac{P_w}{\rho g D} = 4.15 \quad \frac{P_D}{P_w} = 2$$

He	Ar	Liquid	D(cm)	P_w (Nm ⁻²)
■	□	Water	28	11,300
▲	△	Meriam	14	16,700

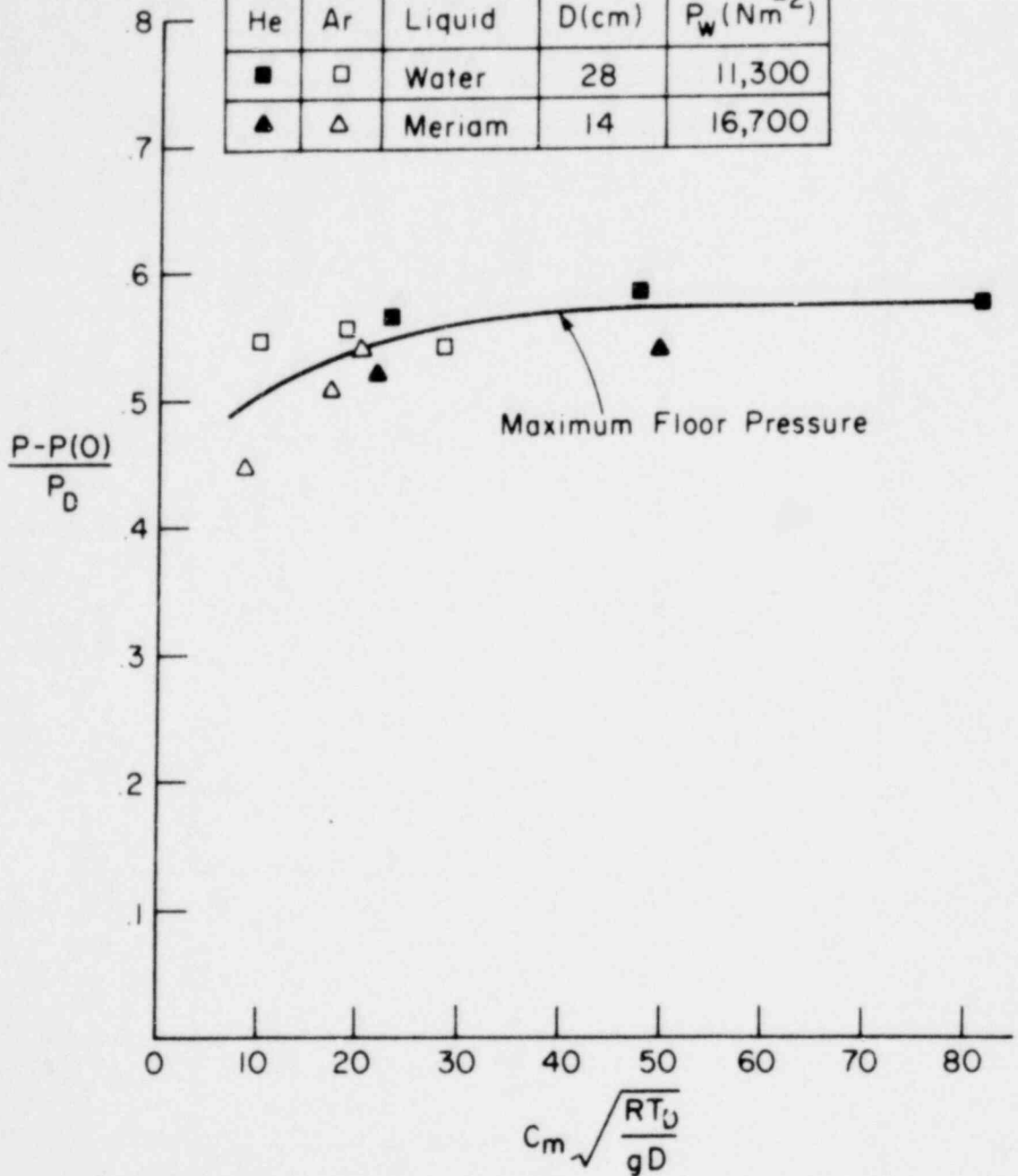


FIGURE 15. First peak in floor pressure versus π_4 .

885 2571

1776 267

$$\gamma = 1.67 \quad \frac{P_w}{\rho g D} = 4.15 \quad \frac{P_D}{P_w} = 3$$

He	Ar	Liquid	D(cm)	$P_w(Nm^{-2})$
■	□	Water	28	11,300
▲	△	Meriam	14	16,700

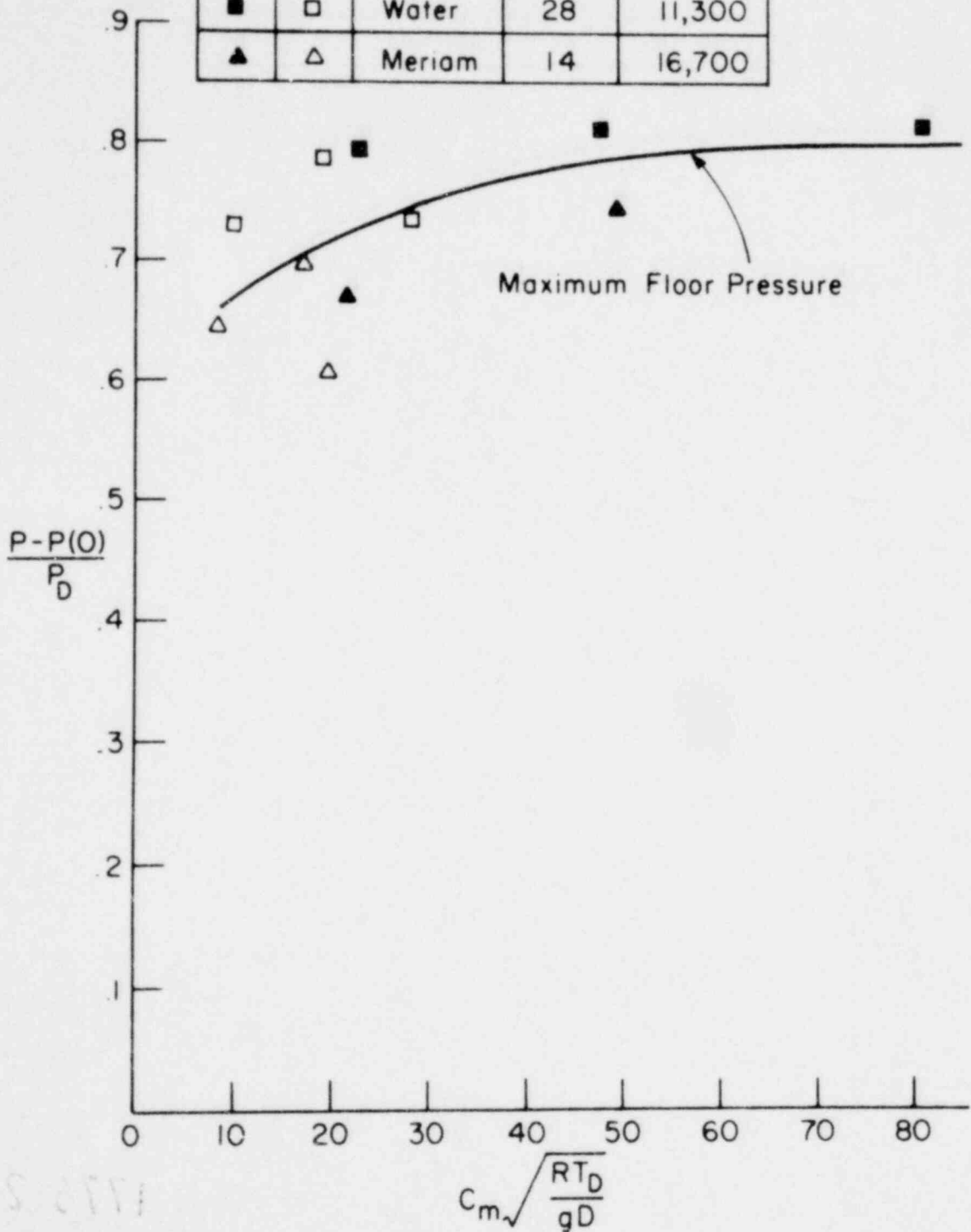


FIGURE 16. First peak in floor pressure versus $C_m \sqrt{\frac{RT_D}{gD}}$

1774 748

$$\gamma = 1.67 \quad \frac{P_w}{\rho g D} = 8.29 \quad \frac{P_D}{P_w} = 3$$

He	Ar	Liquid	D(cm)	P_w (Nm ⁻²)
■	□	Water	28	22,700
▲	△	Meriam	14	33,300

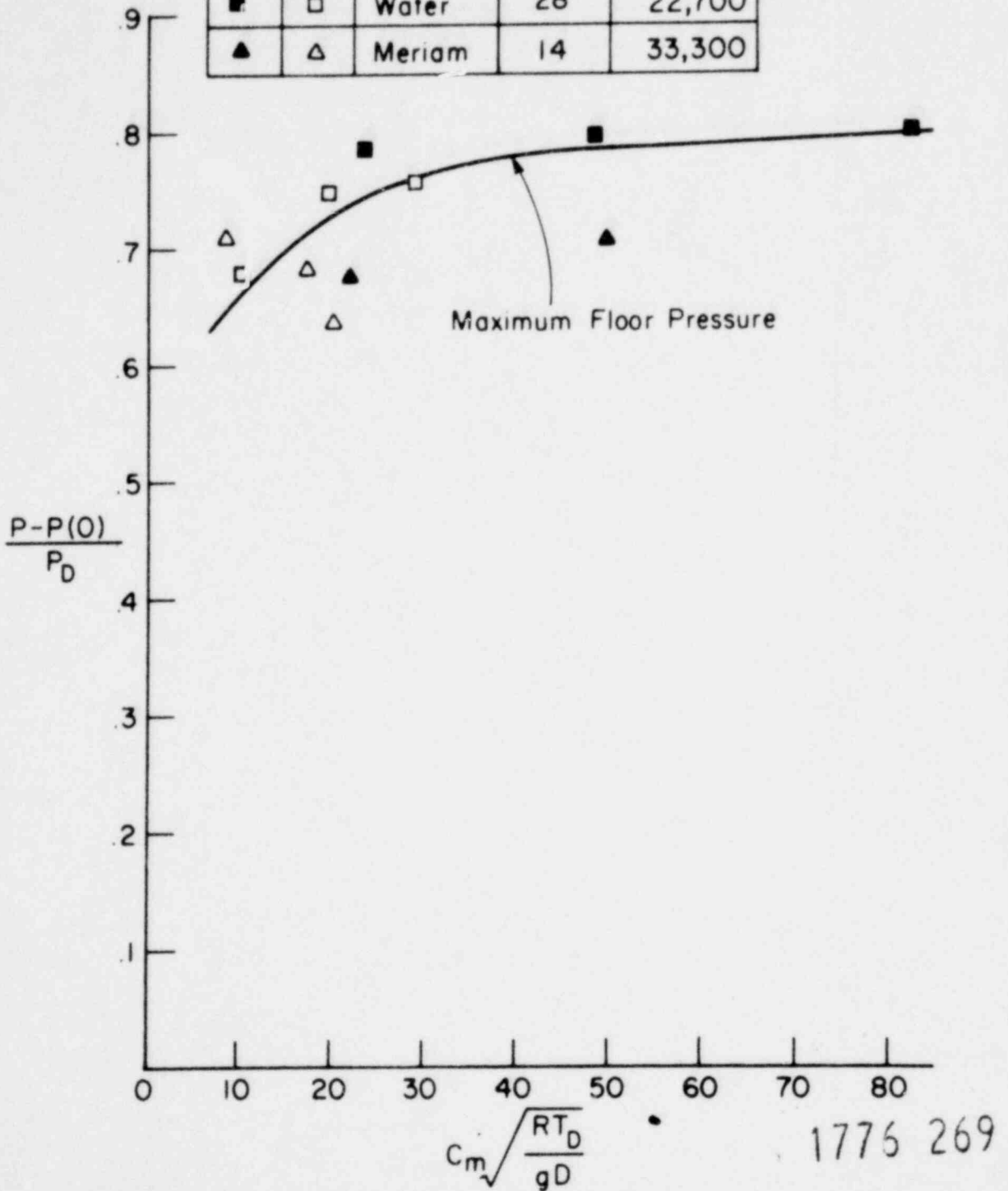


FIGURE 17. First peak in floor pressure versus π_4 .

$$\gamma = 1.67 \quad \frac{P_w}{\rho g D} = 4.15 \quad \frac{P_D}{P_w} = 2$$

He	Ar	Liquid	D(cm)	P_w (Nm ⁻²)
●	○	Water (Ice Bath)	14	5,670
■	□	Water (Ice Bath)	28	11,300
▼	▽	Water (Room Temp)	55	22,100
▲	△	Meriam (Room Temp)	14	16,700

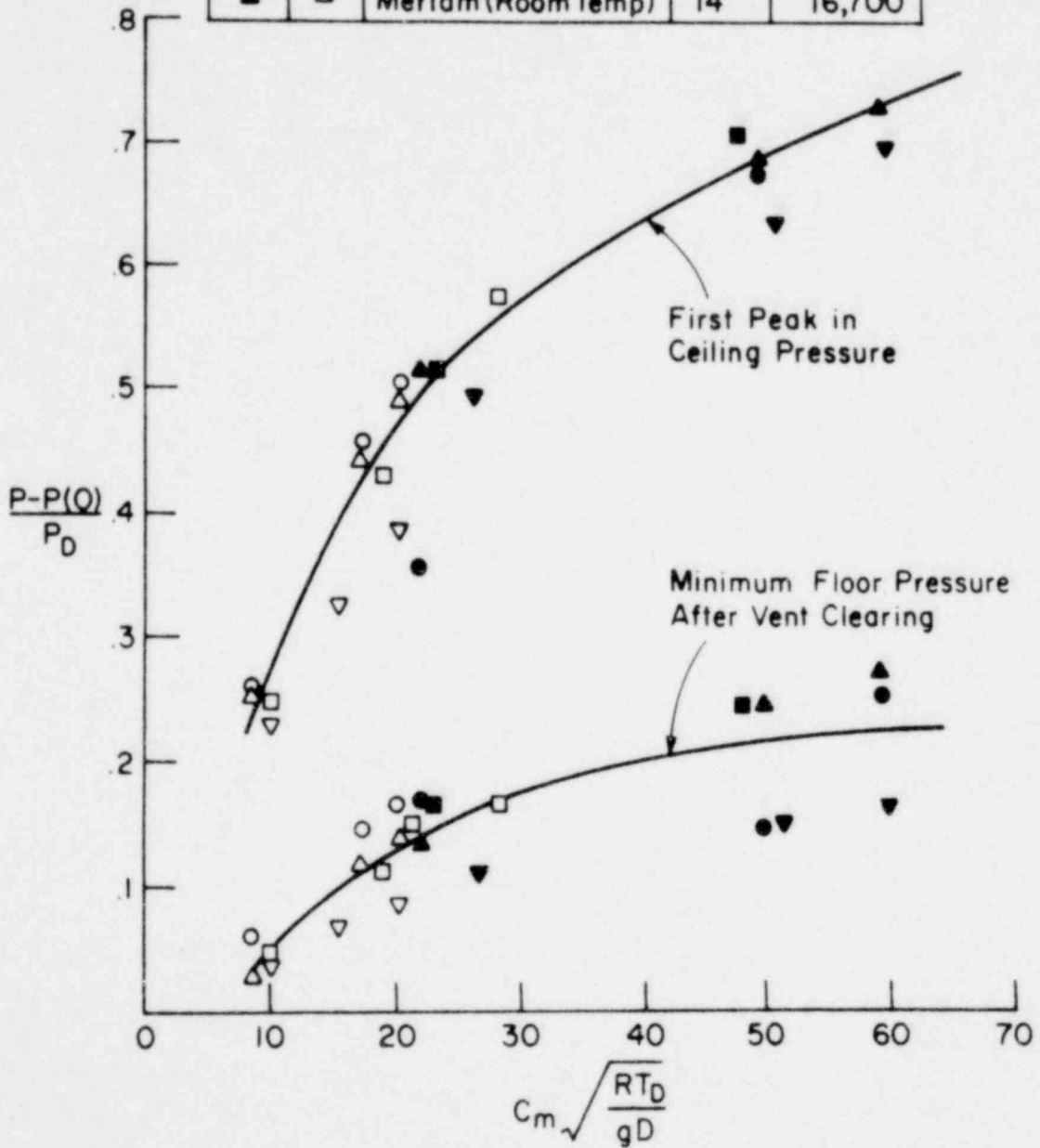


FIGURE 18. First peak in wetwell ceiling pressure and minimum floor pressure as functions of π_4 .

$$\gamma = 167 \quad \frac{P_w}{\rho g D} = 4.15 \quad \frac{P_D}{P_w} = 3$$

He	Ar	Liquid	D(cm)	P_w (Nm ⁻²)
●	○	Water (Ice Bath)	14	5,670
■	□	Water (Ice Bath)	28	11,300
▼	▽	Water (Room Temp)	55	22,100
▲	△	Meriam (Room Temp)	14	16,700

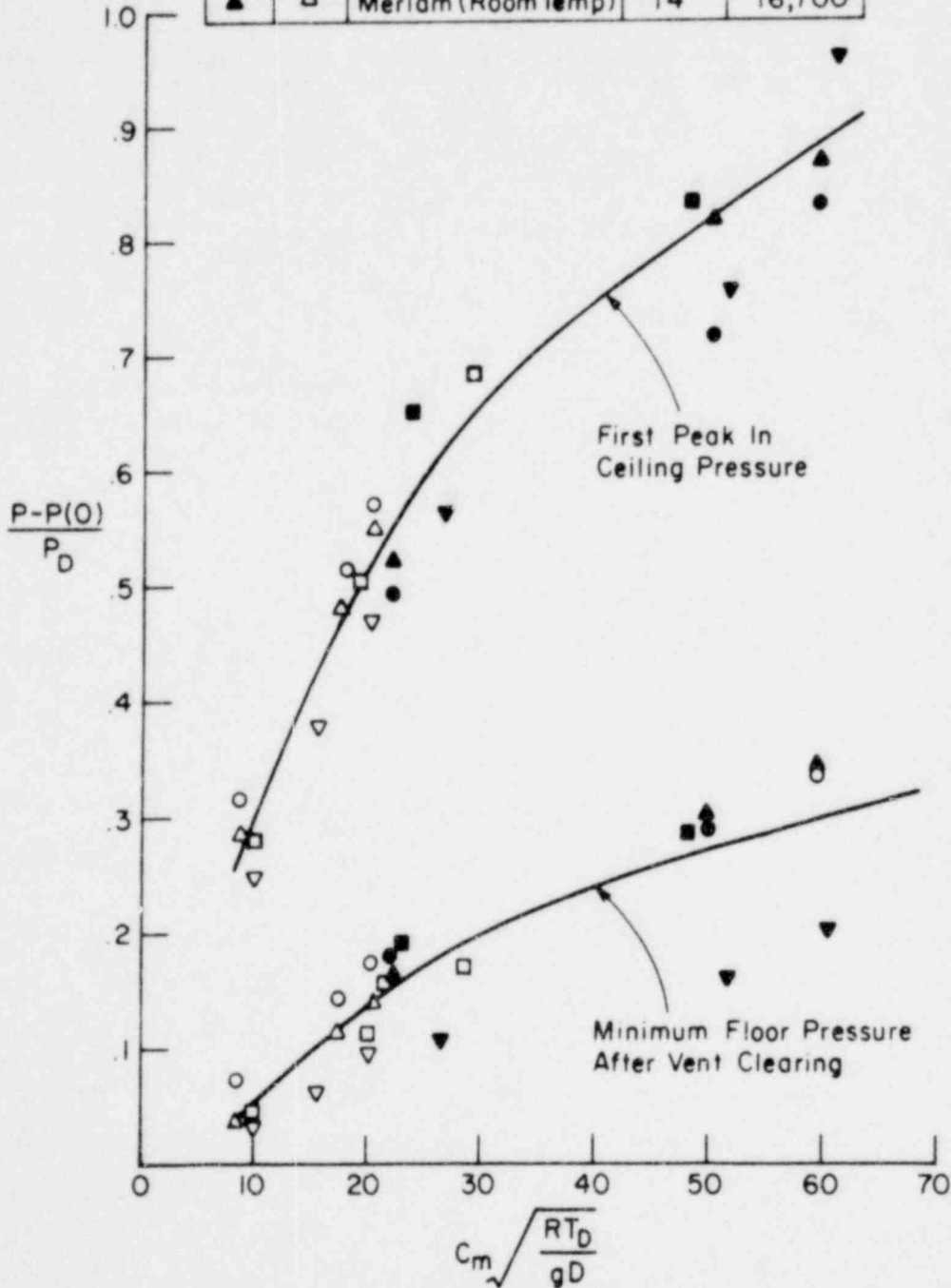


FIGURE 19. First peak in wetwell ceiling pressure and minimum floor pressure as functions of π_4 .

013 2711

1776 271

$$\gamma = 1.67 \quad \frac{P_w}{\rho g D} = 8.29 \quad \frac{P_D}{P_w} = 3$$

He	Ar	Liquid	D(cm)	P_w (Nm ⁻²)
●	○	Water (Ice Bath)	14	11,300
■	□	Water (Ice Bath)	28	22,700
▲	△	Meriam (Room Temp)	14	33,300

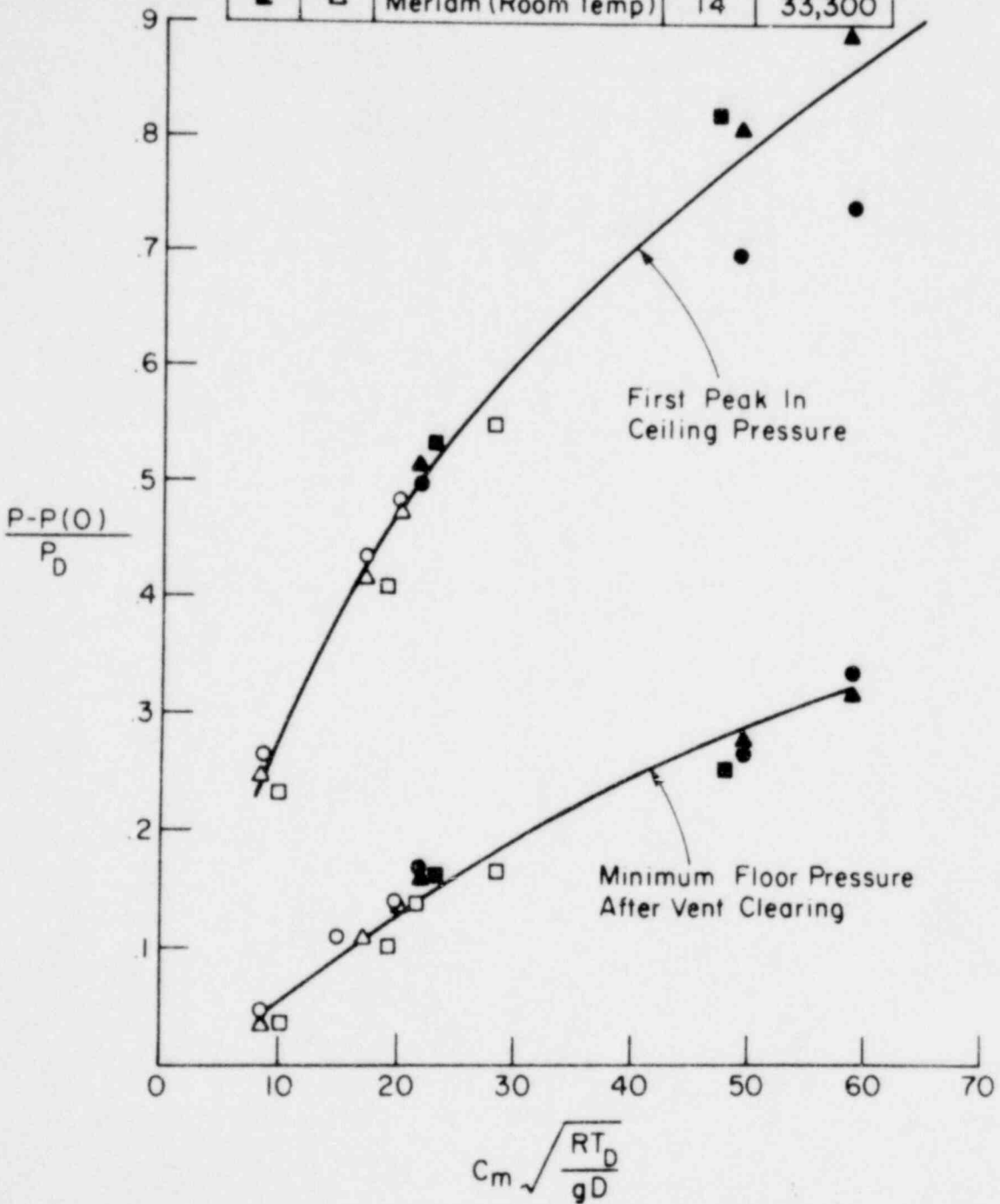


FIGURE 20. First peak in wetwell ceiling pressure and minimum floor pressure as functions of C_m .

$$\gamma = 1.67 \quad \frac{P_w}{\rho g D} = 4.15 \quad \frac{P_D}{P_w} = 2$$

He	Ar	Liquid	D(cm)	P_w (Nm ⁻²)
●	○	Water	14	5,670
■	□	Water	28	11,300
▼	▽	Water	55	22,100
▲	△	Meriam	14	16,700

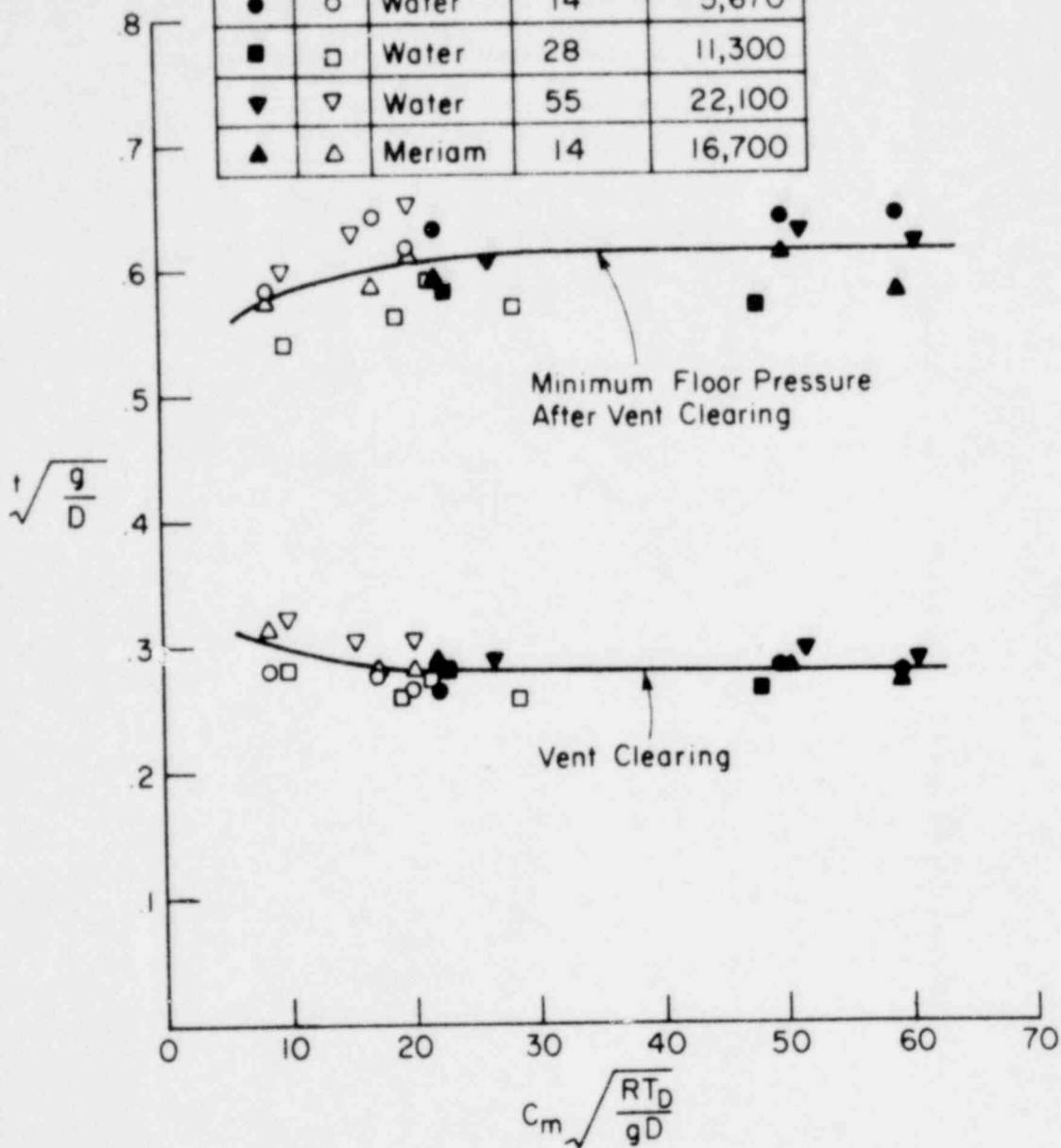


FIGURE 21. Dimensionless times versus π_4 .

1776 273

515 2511

$$\gamma = 1.67 \quad \frac{P_w}{\rho g D} = 4.15 \quad \frac{P_D}{P_w} = 2$$

He	Ar	Liquid	D(cm)	$P_w(Nm^{-2})$
●	○	Water	14	5,670
■	□	Water	28	11,300
▼	▽	Water	55	22,100
▲	△	Meriam	14	16,700

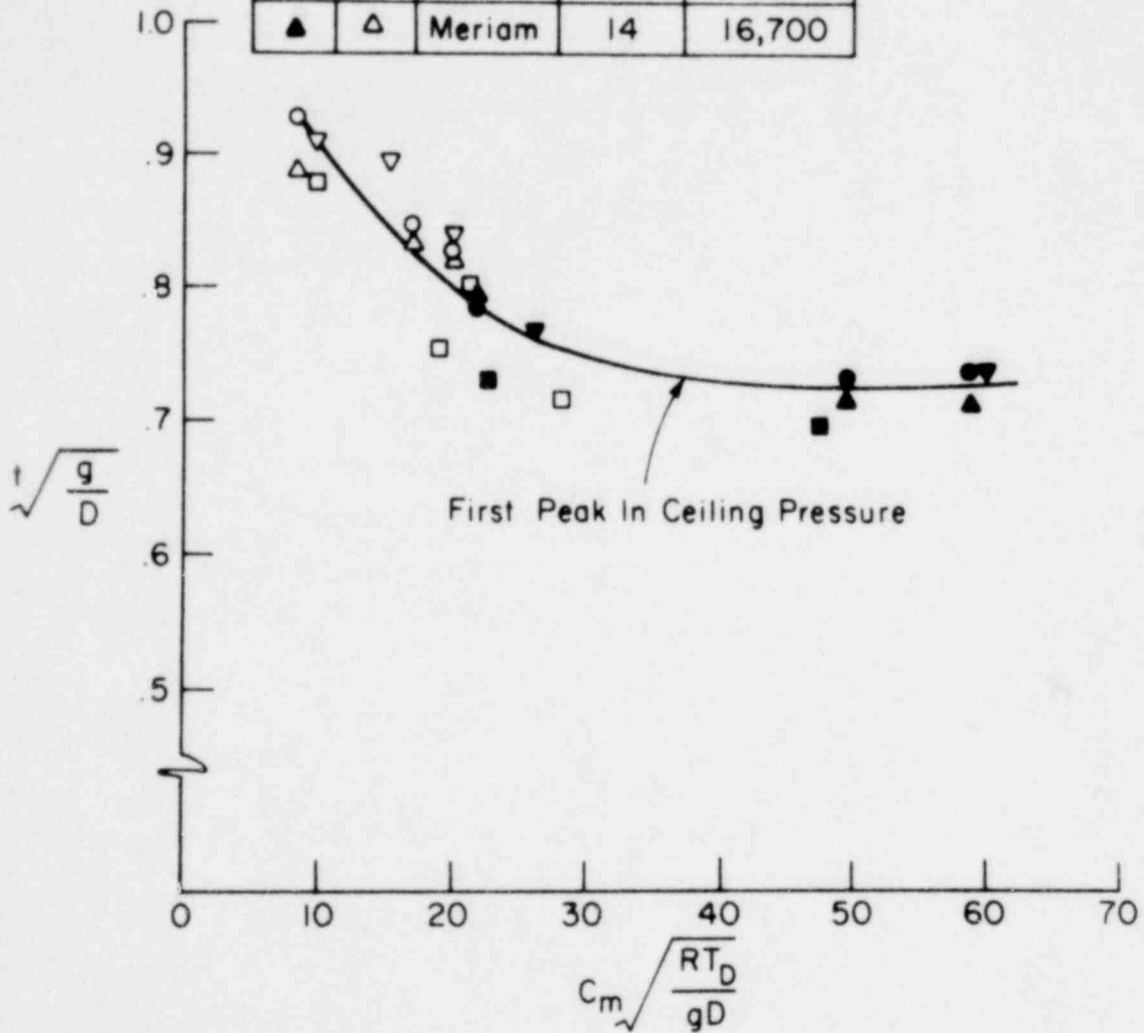


FIGURE 22. Dimensionless time versus π_4 .

1776 274

$$\gamma = 1.67 \frac{P_w}{\rho g D} = 4.15 \quad \frac{P_D}{P_w} = 3$$

He	Ar	Liquid	D(cm)	P_w (Nm ⁻²)
●	○	Water	14	5,670
■	□	Water	28	11,300
▼	▽	Water	55	22,100
▲	△	Meriam	14	16,700

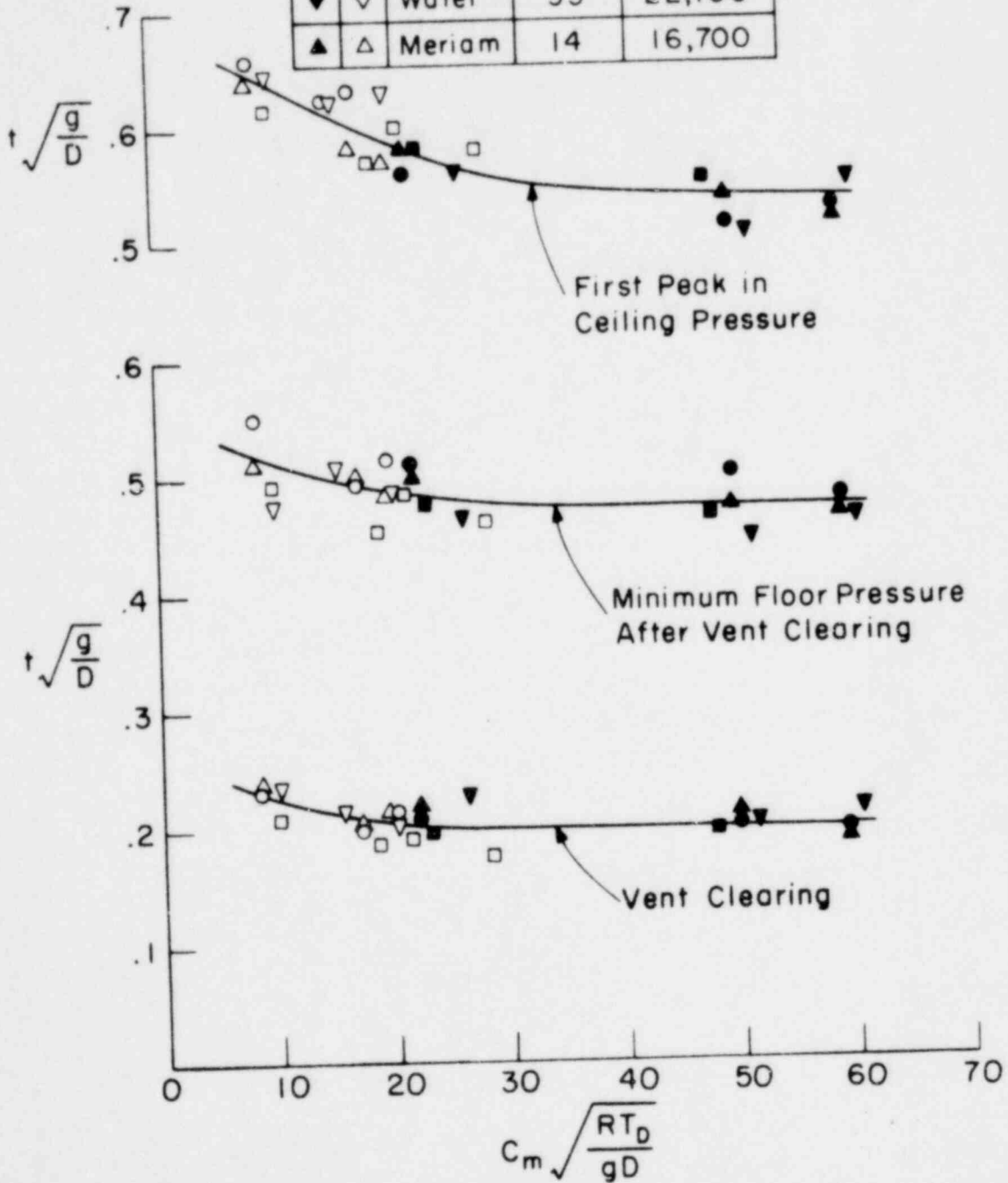


FIGURE 23. Dimensionless times versus π_4 .

1776 275

$$\gamma = 1.67 \frac{P_w}{\rho g D} = 8.29 \quad \frac{P_D}{P_w} = 3$$

He	Ar	Liquid	D(cm)	P_w (Nm ⁻²)
●	○	Water	14	11,300
■	□	Water	28	22,700
▲	△	Meriam	14	33,300

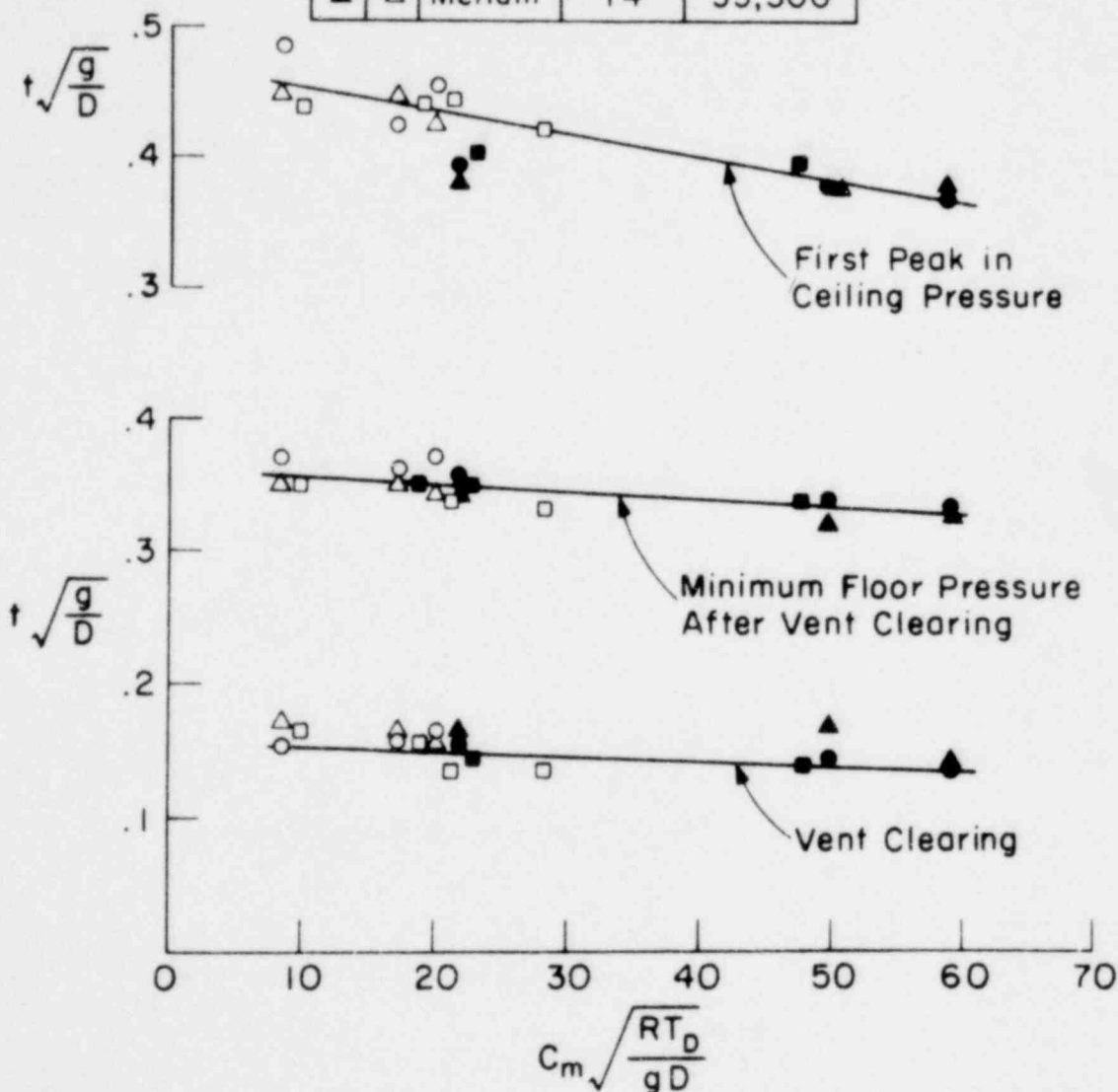


FIGURE 24. Dimensionless times versus π_4 .

1776 276

115 277

$$\gamma = 1.4 \quad \frac{P_w}{\rho g D} = 4.15 \quad \frac{P_D}{P_w} = 3$$

Air/Water	D (cm)	P_w (Nm ⁻²)
○	14	5670
□	28	11,330
▽	55	22,100

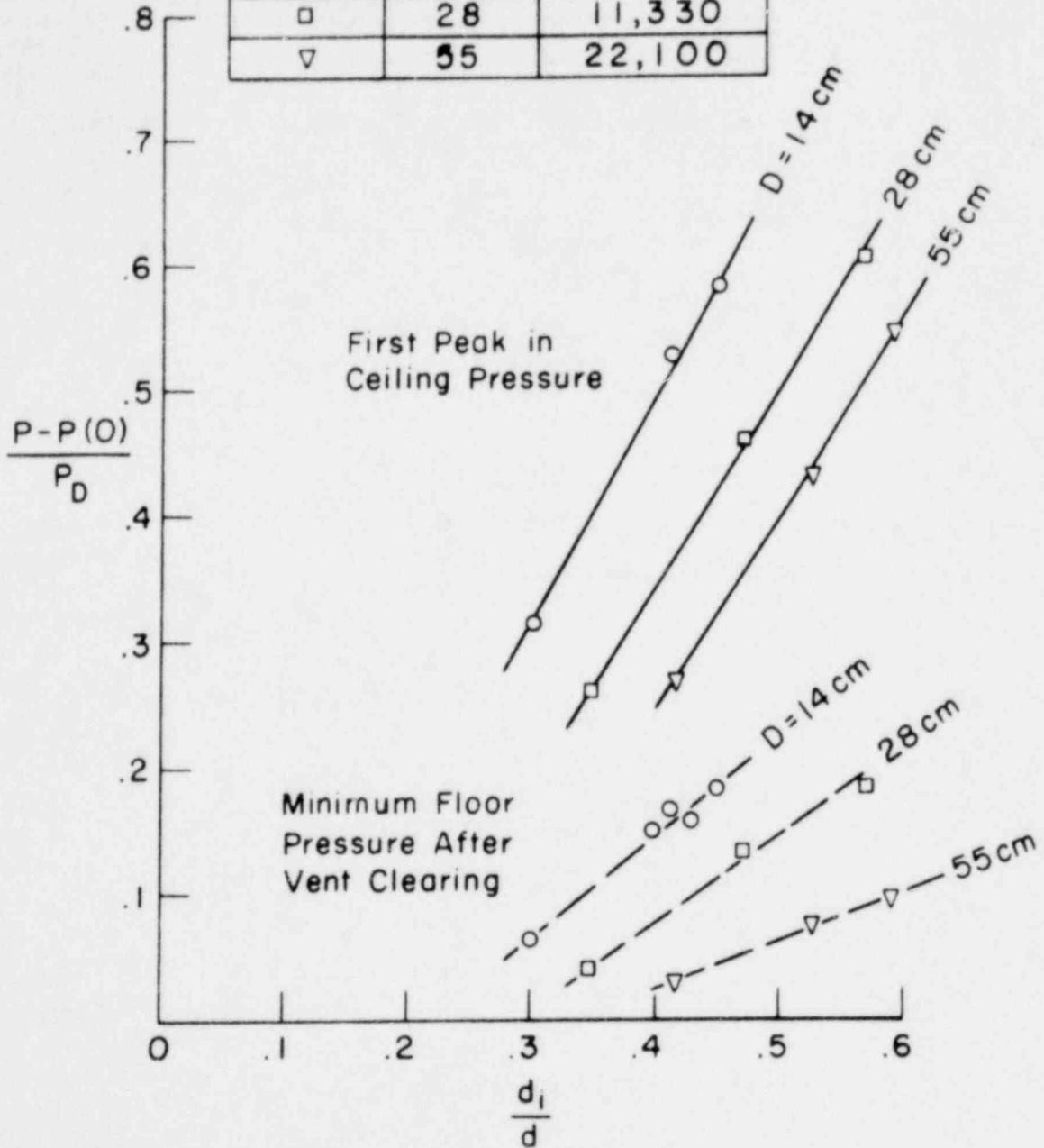


FIGURE 25. First peak in ceiling pressure and minimum floor pressure as functions of d_1/d .

$$\gamma = 1.67 \quad \frac{P_w}{\rho g D} = 4.15 \quad \frac{P_D}{P_w} = 3$$

He/Water	Ar/Water	D (cm)	P_w (Nm ⁻²)
●	○	14	5 670
■	□	28	11,330
▼	▽	55	22,100

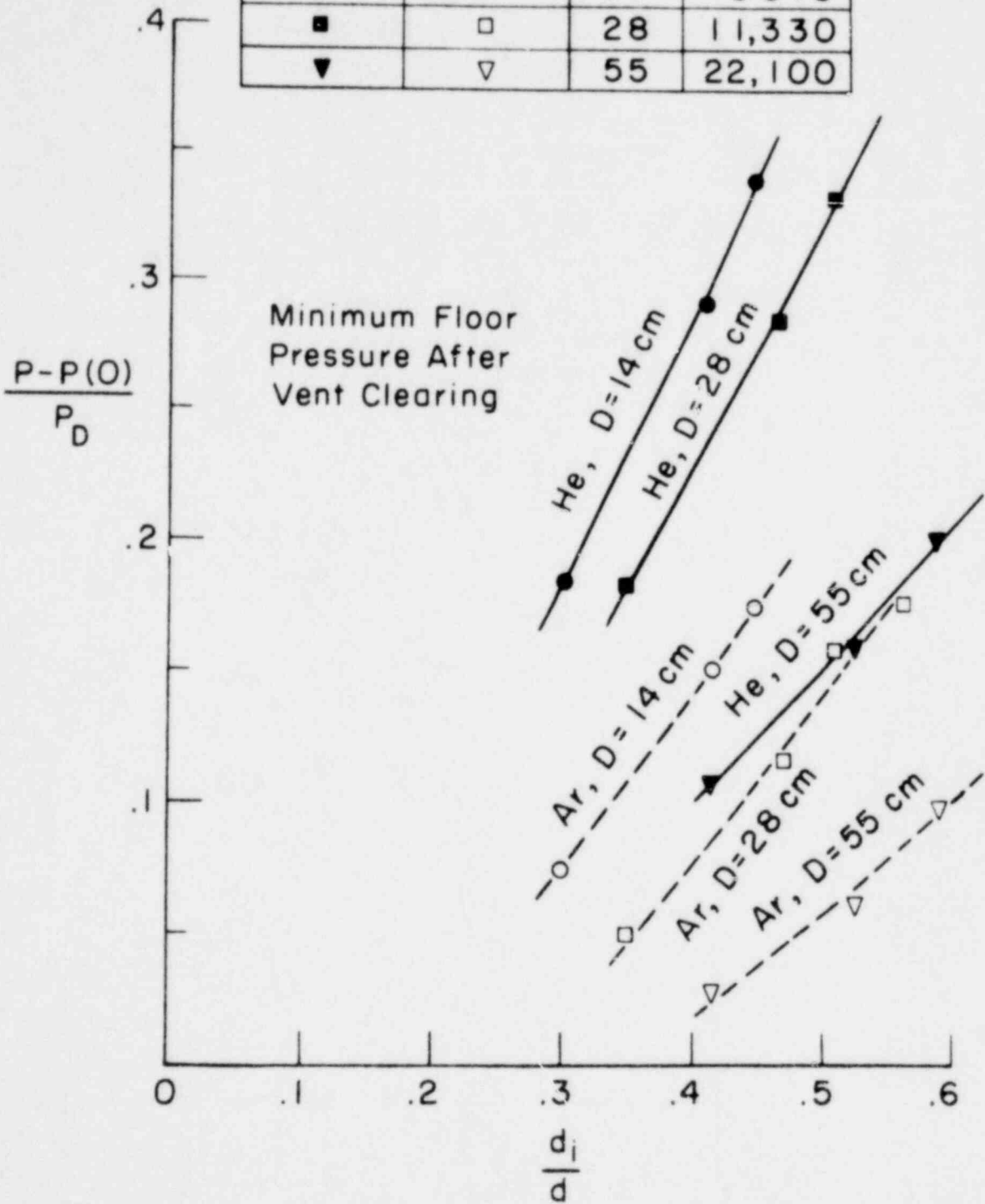


FIGURE 26. Minimum floor pressure versus d_i/d .

1776 278

PTC 2111

$$\gamma = 1.67 \quad \frac{P_w}{\rho g D} = 4.15 \quad \frac{P_0}{P_w} = 3$$

He/Water	Ar/Water	D (cm)	P_w (Nm ⁻²)
●	○	14	5 670
■	□	28	11,330
▼	▽	55	22,100

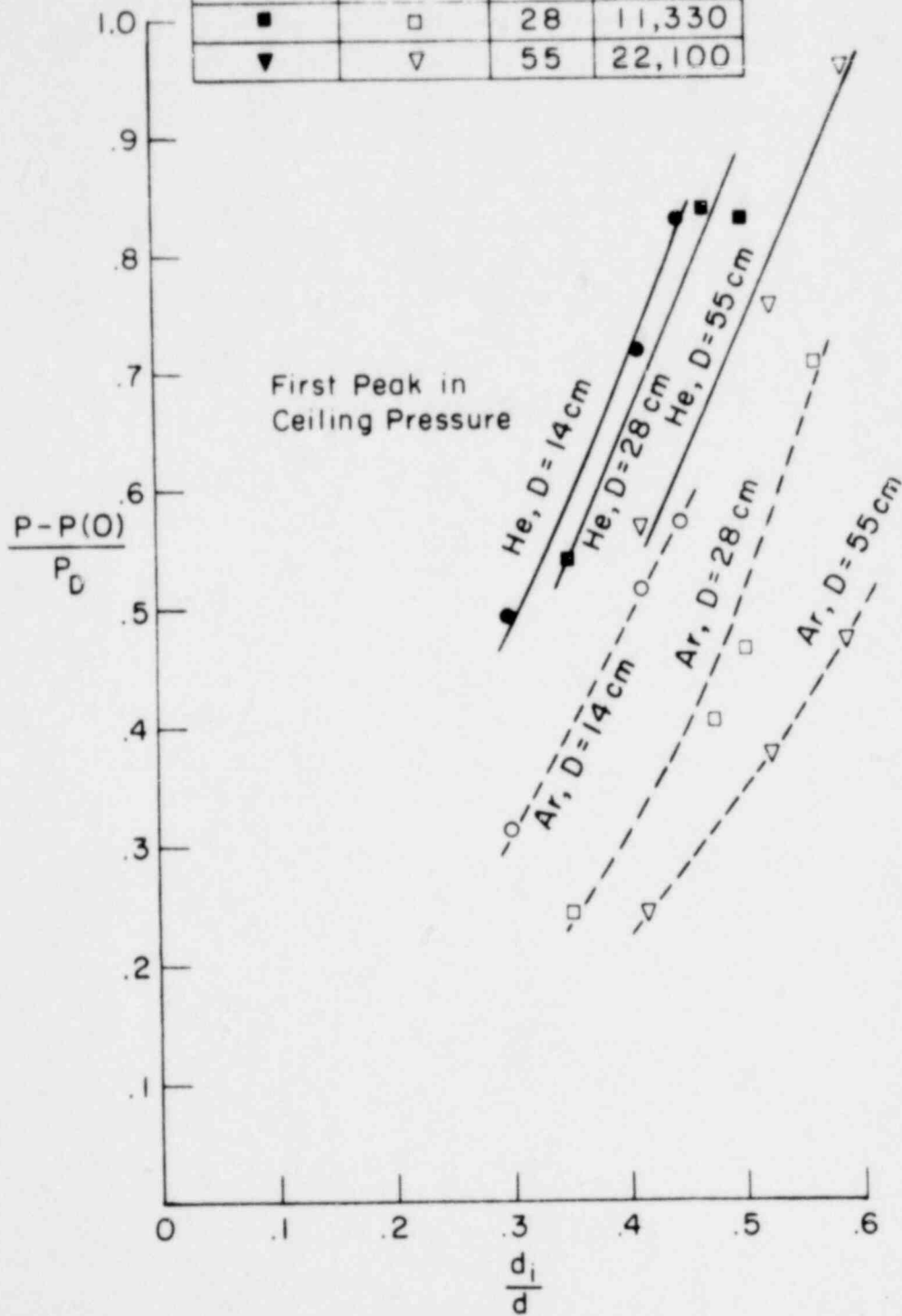


FIGURE 27. First peak in ceiling pressure versus d_i/d .

875 8771

1776 279

$$\gamma = 1.4 \quad \frac{P_w}{\rho g D} = 4.15 \quad \frac{P_D}{P_w} = 2$$

Air	Liquid	D(cm)	$P_w(Nm^{-2})$
○	Water (Ice Bath)	14	5,670
●	Water (Room Temp)	14	5,670
□	Water (Ice Bath)	28	11,300
■	Water (Room Temp)	28	11,300
▼	Water (Room Temp)	55	22,100
△	Meriam (Room Temp)	14	16,700

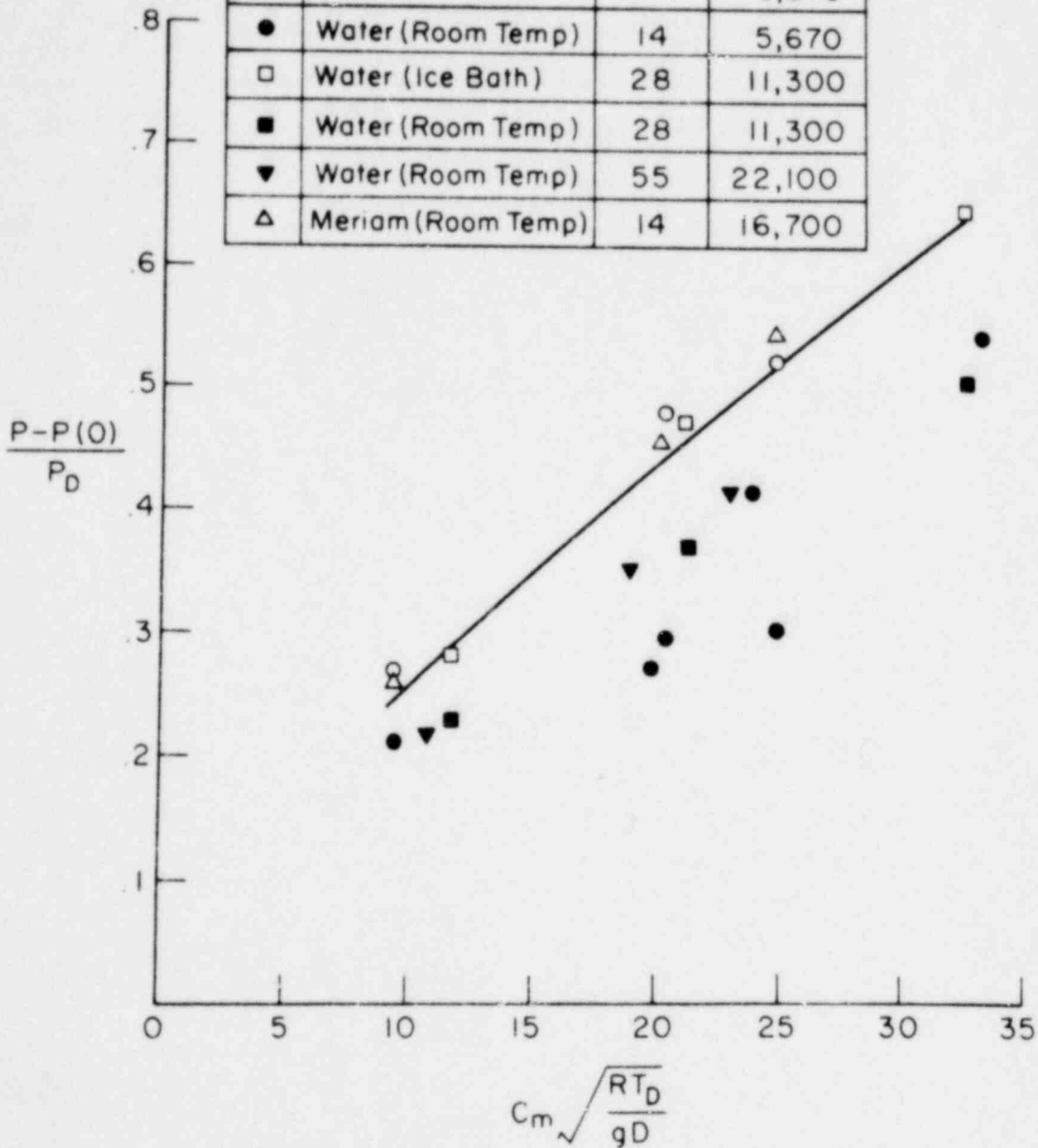


FIGURE 28. Vapor pressure effect on first peak in ceiling pressure.

185-2557

1776 280

$$\gamma = 1.67 \quad \frac{P_w}{\rho g D} = 4.15 \quad \frac{P_D}{P_w} = 2$$

He/Ar	Liquid	D(cm)	P_w (Nm ⁻²)
○	Water (Ice Bath)	14	5,670
●	Water (Room Temp)	14	5,670
□	Water (Ice Bath)	28	11,300
■	Water (Room Temp)	28	11,300
▼	Water (Room Temp)	55	22,100
△	Meriam (Room Temp)	14	16,700

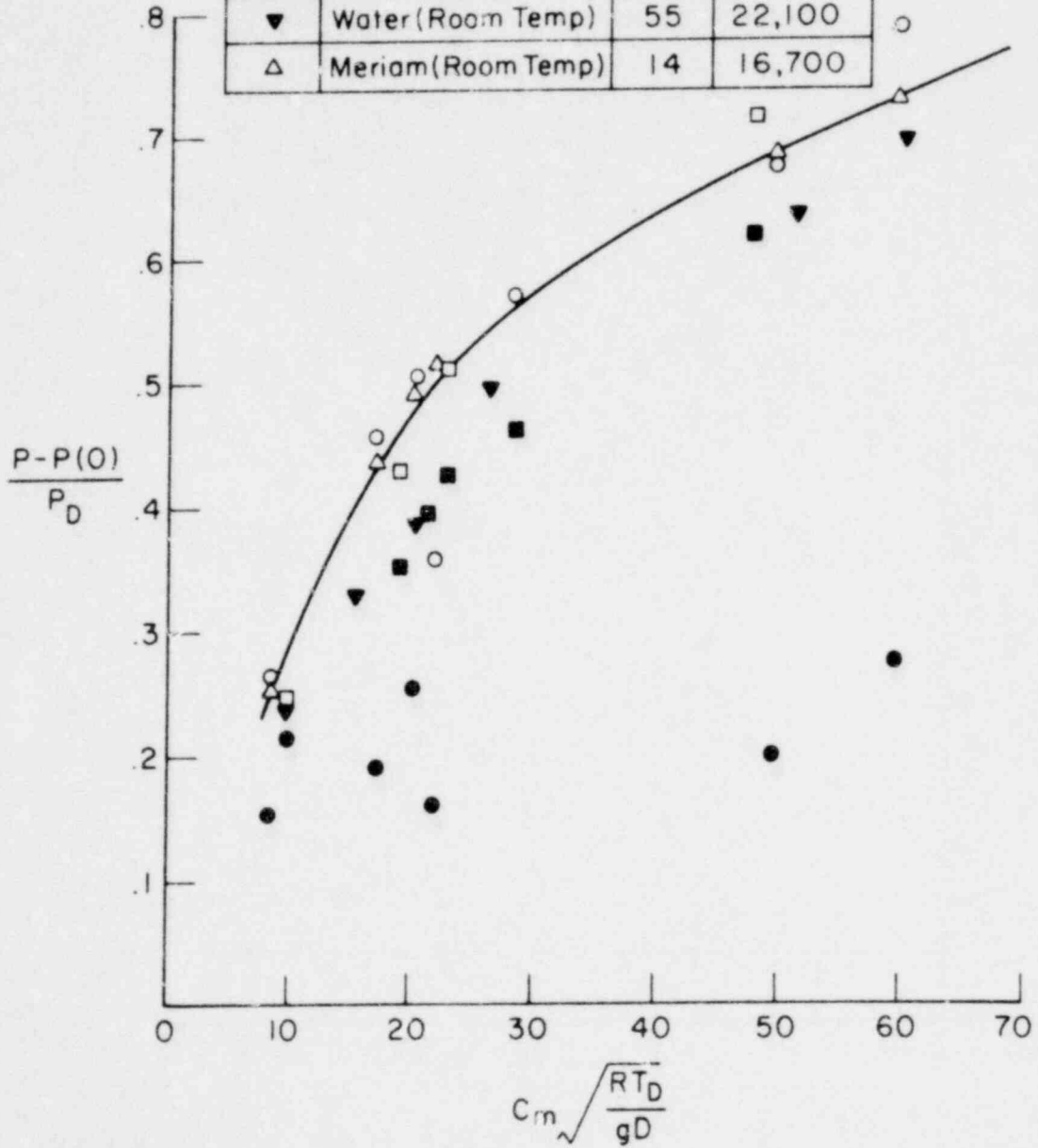


FIGURE 29. Vapor pressure effect on first peak in ceiling pressure.

085 2517

1775 281

$$\gamma = 1.67 \quad \frac{P_w}{\rho g D} = 8.29 \quad \frac{P_D}{P_w} = 3$$

He/Ar	Liquid	D(cm)	P_w (Nm ⁻²)
○	Water (Ice Bath)	14	11,300
●	Water (Room Temp)	14	11,300
□	Water (Ice Bath)	28	22,700
■	Water (Room Temp)	28	22,700
△	Meriam (Room Temp)	14	33,300

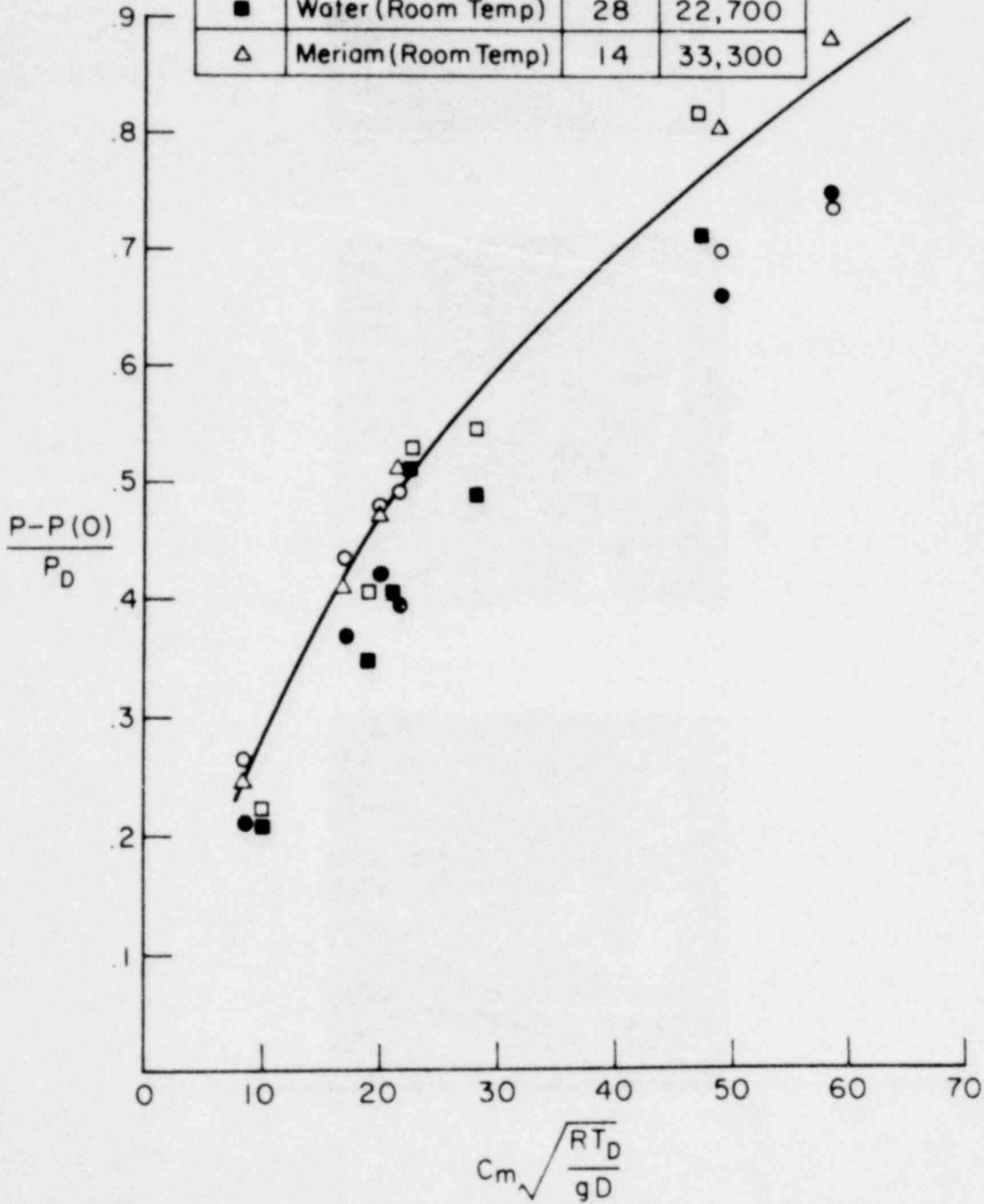


FIGURE 30. Vapor pressure effect on first peak in ceiling pressure.

1776 282

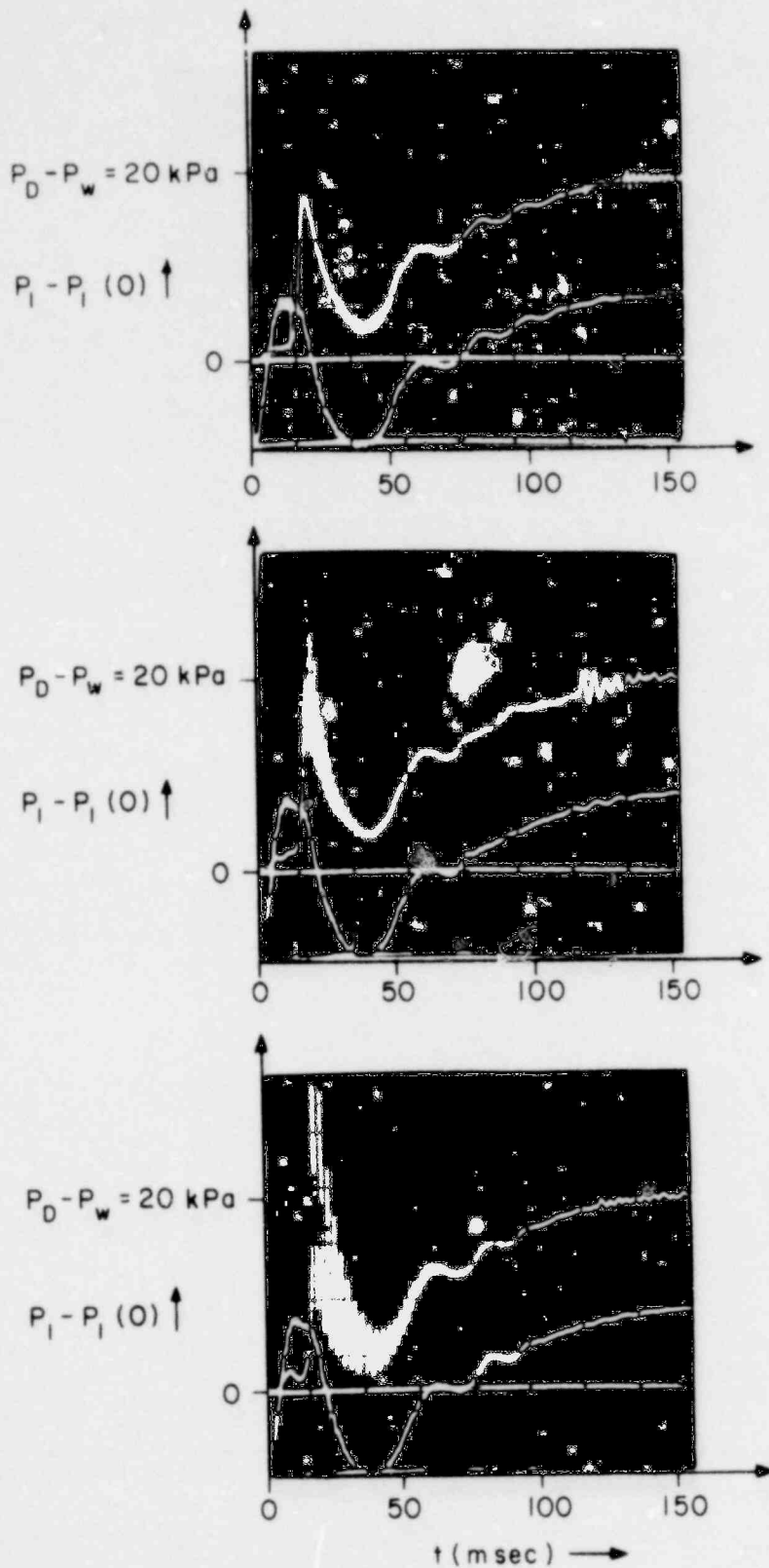


FIGURE 31. Pressure histories in a sequence of tests where oil was used as the wetwell liquid (air/oil, $D = 14 \text{ cm}$, $\pi_1 = 1.4$, $\pi_2 = 8.29$, $\pi_3 = 3$, $\pi_4 = 25.1$).

S85 2511

1775 283

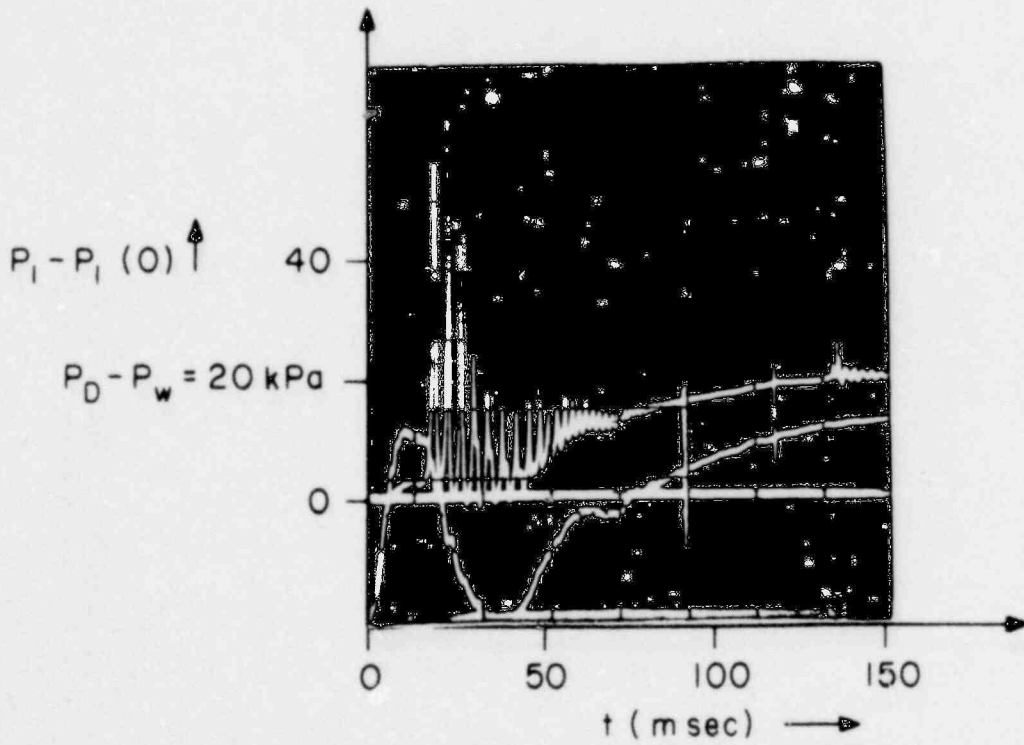
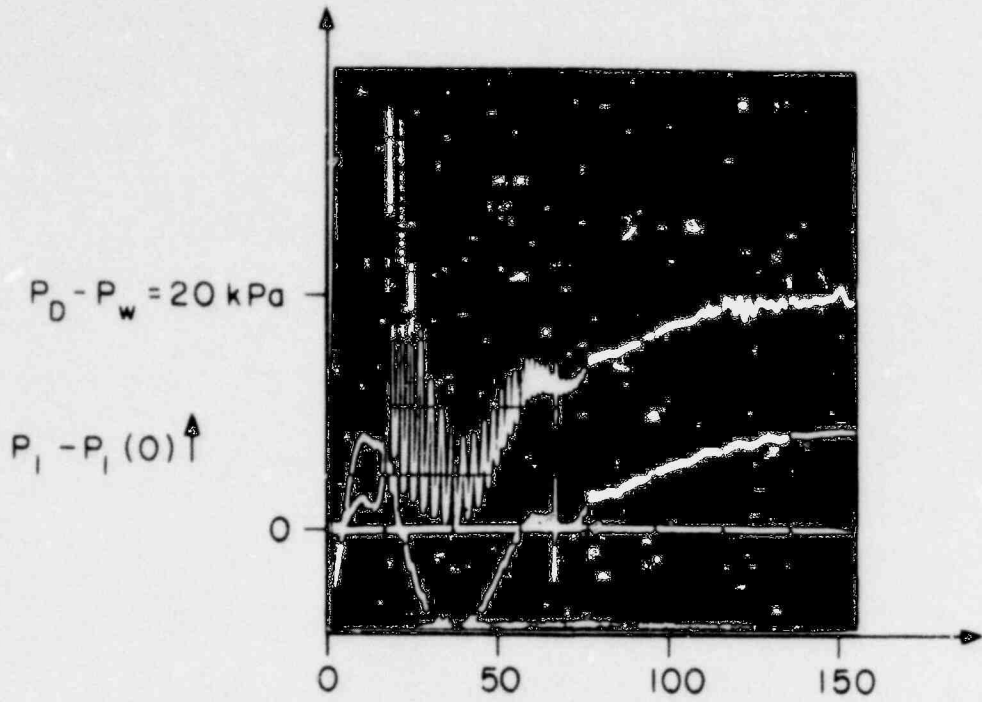


FIGURE 31. Continued.

1776 284

UNITED STATES
NUCLEAR REGULATORY COMMISSION
WASHINGTON, D. C. 20555

OFFICIAL BUSINESS
PENALTY FOR PRIVATE USE, \$300

POSTAGE AND FEE PAID
U.S. NUCLEAR REGULATORY
COMMISSION



1776 285